Integrated Circuit and System Design for Wireless Biosignal Monitoring

Timothy David Morrison

A dissertation
submitted in partial fulfillment of the
requirements for the degree of

Doctor of Philosophy

University of Washington

2017

Reading Committee:

Brian Otis, Chair

Robert Darling

Shwetak Patel

Program Authorized to Offer Degree:
Electrical Engineering

University of Washington

Abstract

Integrated Circuit and System Design for Wireless Biosignal Monitoring

Timothy David Morrison

Chair of the Supervisory Committee:
Professor Brian Otis
Department of Electrical Engineering

This document presents various techniques and systems for recording biological signals. Specifically electrocardiography (ECG), electromyography (EMG) and single-unit neuron recording applications are discussed. These recording techniques sense electrical potentials generated by biological functions which are then amplified and sampled using electronic devices. The evolution of this biosignal monitor electronic device over four design generations highlights the advantages of utilizing integrated circuits (ICs) designed solely for the given application. The final design combines the benefits of a low power IC and the highly customizable nature of a microconroller. Thanks to its high level of customizability after fabrication this system is ideal for innumerable applications in the field of biosignal monitoring by lowering the technically barrier and development time required for many future biosignal monitoring applications.

TABLE OF CONTENTS

LIST OF FIGURES

LIST OF TABLES

DEDICATION

To my parents.

Chapter 1

INTRODUCTION

The advancement of medical science requires a steady stream of new knowledge of biological systems. For something to be understood the first step is observing and recording the behavior. This need for new data is very complimentary to the strengths of electronic devices. From a distance it may seem that biological organisms have little in common with the field of electronics but they in fact share a surprising amount. Biological organisms use electrical signaling throughout to control key systems, from collecting sensory information to controlling locomotion. Using electrodes the electrical signals output can be measured, recorded and processed electronically. With properly designed devices specifically targeted at the biosignal monitoring space we can have a significant impact on the progression of medical science, from understanding basic signaling within the brain of laboratory animals to providing early-warning of potentially life-threatening diseases in humans.

In this document we will mainly focus on two major areas of medical research using electronic monitoring devices, small-animal research using *in vivo* recording techniques and human health monitoring with non-invasive external wearable sensors. The scale of these two applications are very different but their functionality is extremely similar, making it possible for one device to thrive in both applications. Table 1.1 compares a few common biosignals and their signal characteristics.

In the medical and scientific research communities there are existing devices currently deployed in relatively small numbers in animal research laboratories but these devices are mostly bulky which limits the number of applications they're suited for. Recording biosignals from freely moving small animals, such as mice, requires a self-contained device capable of

Table 1.1: Comparison of common biosignals.

Signal	**Voltage Range**	**Frequency Range (Hz)**	**Sensed Biological Activity**
ECG	0.1 - 5 mV	0.1 - 150	Heart
EMG	10 μV - 50 mV	10 - 1 k	Muscle
EEG	10 - 100 μV	0.5 - 100	Brain
Single-Unit	0.1 μV - 100 mV	300 - 5 k	Neural

amplifying the desired signal(s) and transmitting this data to a display. Not only must this device be small and light enough for the animal to carry, it must be easily operated so the researcher can concentrate on the experiment at hand instead of on the recording device itself.

Human wearable devices are not nearly as space constrained from a technical perspective. A human is capable of carrying a device orders of magnitude heavier than a mouse, for example. However, a practical reality is humans ultimately will decide if they will use a device or not, where as a laboratory animal does not get to make this choice. If humans will not willingly use a device, because it is too bulky or encumbering, then the device has no real value for the general populace. Because of this it is just as important that medical devices for humans be as small as possible so they are unnoticeable during everyday life.

Chapter 2 will start the discussion of medical devices targeted at human use for electromyography (EMG) to detect muscle activity. The first design uses commercially available components. It is capable of recording two independent EMG channels and transmitting the data wirelessly to a paired USB-enabled receiver, eventually offloading the data to a connected PC. The device is well suited for its application in a clinical setting but is fairly large in size. It will be shown that the main contributor to this size is its battery. Reducing

the battery size itself is not sufficient without design changes since reduced lifetime is highly undesirable. Significant power savings can be accomplished by creating a custom integrated circuit (IC) that is specially designed for low-power medical monitoring. The second design, a single channel EMG monitor with wireless transmitter, demonstrates this with an order of magnitude reduction in size.

Next, in Chapter 3, we present a 4-channel wireless biosignal monitor using a new IC design. This device targets both neural recording in laboratory mice as well as human heart monitoring via electrocardiography (ECG). These two recording modalities are performed by the same chip using its variable-gain amplifiers to configure each sensor channel for one or the other. While the device itself was highly successful in these applications it suffers from hard-wired functionality. The device can only sample from the 4 channels and wirelessly transmit at 100% duty-cycle. For other applications with different sampling/transmitting needs a new IC with logic specific to their requirements would need to be designed.

Finally, Chapter 4 introduces an IC designed to record up to 12 biosignals in parallel while transmitting all data wirelessly. The key differentiator of this circuit, aside from the increase in recording channels, is its ability to mate with an external microcontroller. The system itself was designed so all sub-blocks of the circuit can be controlled individually with external signaling. It will be shown that this design technique greatly increases the number of applications the chip is suited for. Due to the highly configurable nature of microcontrollers and easily updated software the device can simply be reworked for new and unique biosignal monitoring applications without requiring a new IC to be designed and fabricated, an extremely time-consuming and difficult process. To demonstrate the versatility of the device it was embedded into a sports shirt along with electrodes to create a 12-lead continuous ECG smart-shirt which can be reprogrammed to act as a low-power heart rate monitor. Electroencephology (EEG) and EMG applications are also discussed.

In Chapter 5 some concluding remarks will summarize the paper's findings and looks towards future work in the field.

Chapter 2

WIRELESS EMG

In humans muscle contraction is instigated from signals initiated inside the brain, traveling through the body via the Central Nervous System (CNS) all the way to the muscle tissue itself. These electrical signals, known as action potentials (AP), use various mechanisms to travel through the body depending on the biological structure but they are, at their core, a movement of charge.

Action potentials are used to directly control human locomotion. When an action potential travels along a muscle fiber it causes that fiber to contract. Electromyography (EMG) is the study of these electrical signals coming from muscle fibers. EMG gives us a way of inferring muscle activity in a purely electronic means by observing their external voltage. Discussed in this chapter are two different non-invasive electronic devices designed to record human EMG signals from the surface of the skin.

2.1 2-Channel Wireless EMG System Using Off-The-Shelf Components

Designed using only off-the-shelf components (i.e. no custom integrated circuits) this 1st generation device was created to record EMG signals from the human forearm. Two EMG recording channels were included so both the extensor and flexor muscle groups could be recorded simultaneously. Signals in this group can range anywhere from $10\,\mu$V to $50\,$mV.

2.1.1 Design

A block diagram of the recording device can be seeing in Figure 2.1. The two EMG signals are first sent to a low-noise Instrumentation Amplifier (IA), then to a second-stage low-power Variable Gain Amplifier (VGA). The first-stage part, a Texas Instruments INA333,

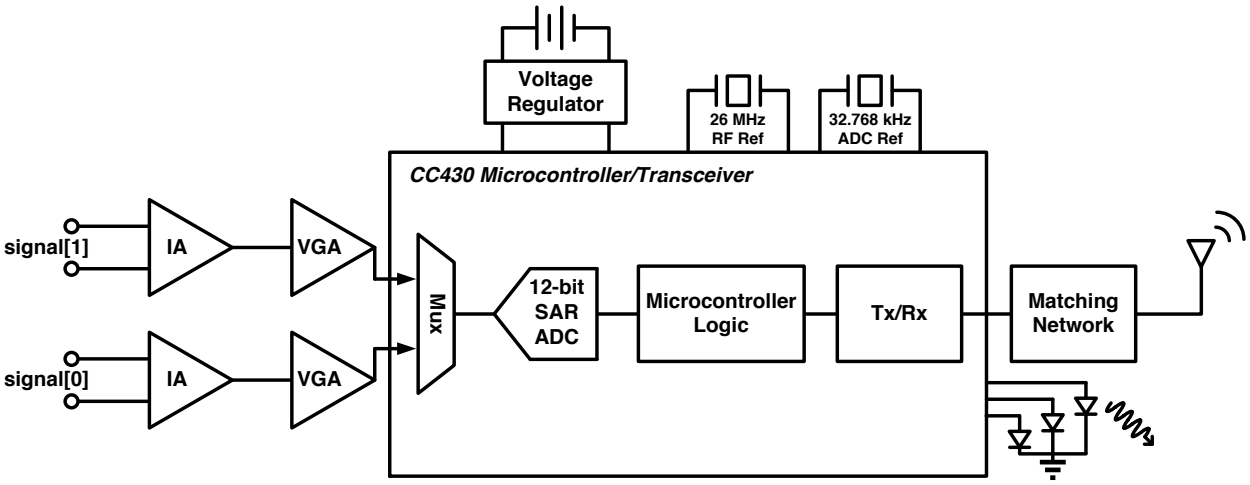

Figure 2.1: Block diagram of the 2 channel wireless EMG sensor and transmitter.

was chosen due primarily due to its low noise and high gain; suitable for boosting up μV-level signals high enough without contributing significant noise to the signal compared to the higher-noise second stage (Texas Instruments OPA333). The second-stage VGA is a simple single-ended resistive-feedback operational amplifier (OpAmp). To vary the gain the feedback resistance value is set via a digitally programmable potentiometer (Microchip MCP4632). Each signal channel is independently programmed allowing for separate gain values for each channel.

The heart of this design is the central microcontroller and wireless transceiver. Both functions are combined on a single chip, the Texas Instruments CC430F5133, which reduces overall size requirements when compared to a two-chip solution. The microcontroller has a built-in 12-bit analog-to-digital converter (ADC) which is used to sample our amplified EMG signals. Since there is only one ADC but we are recording two channels of EMG the input to the ADC must be time-multiplexed to sample both. The microcontroller handles this muxing between channels, switching channels after each ADC sample. Using a 32.768 kHz crystal reference the microcontroller also ensure a consistent sampling rate of 5 ksps is achieved for both channels.

After sampling the EMG waveforms the resulting digital data is then transmitted wirelessly to a paired receiver using the CC430's 915 MHz frequency-shift keying (FSK) transceiver. EMG data is buffered until 83 samples of each channel (166 samples total) have been converted. Once this threshold has been reached a digital packet is created by appending this data to a start-of-packet 16-bit "sync word" and an 8-bit packet counter which increments after every packet transmission. Figure 2.2 shows the full wireless data packet construction.

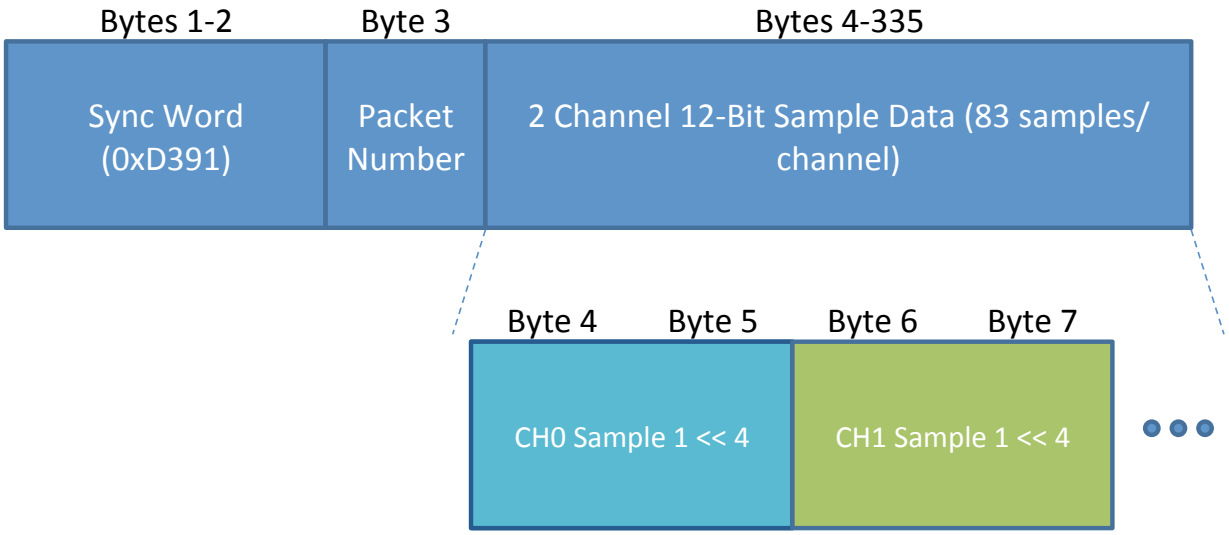

Figure 2.2: Wireless packet structure of transmitted EMG data.

The CC430 microcontroller is connected to a 2-channel digital potentiometer via I^2C. When the user wants to change the gain of any EMG channel they simply send a wireless command to the device. The EMG sensing device will then receive the command and change the potentiometer appropriately to achieve the desired gain. The wireless command is send from the custom-designed receiver that also utilizes a CC430 with its wireless transceiver. This receiver board is connected to a PC via USB and accepts gain adjustment commands over the USB interface. Directly after a valid packet from an EMG sensor is received the receiver board will switch from receive (Rx) to transmit (Tx) mode and send the request for

new EMG gain(s). Likewise, directly after the EMG sensor finishes sending a data packet it will transition from Tx to Rx mode to listen for any commands. Once the EMG sensor has enough data to send a new data packet it will switch back to Tx mode.

The full schematic of the EMG sensor device can be seen in Figure 2.3. The CC430 itself requires many components so it has been shown as a simplified green box to aid in readability. The details of the CC430 implementation, along with the RF matching network and antenna, can be seen in Figure 2.4.

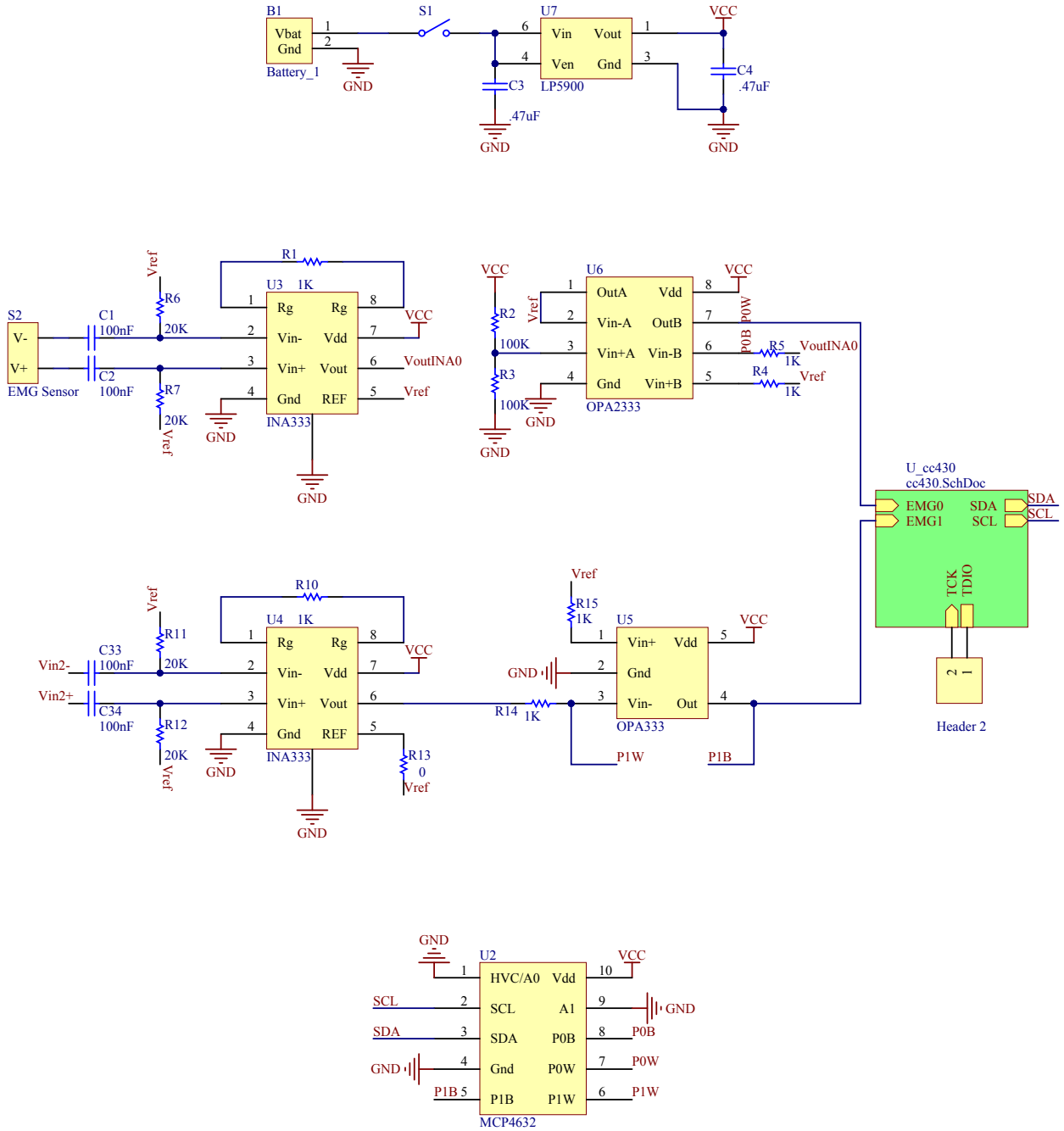

Figure 2.3: Schematic of the 2 channel wireless EMG system PCB. The Texas Instruments CC430 chip implementation is noted in the green box. A detailed schematic can be seen in Figure 2.4

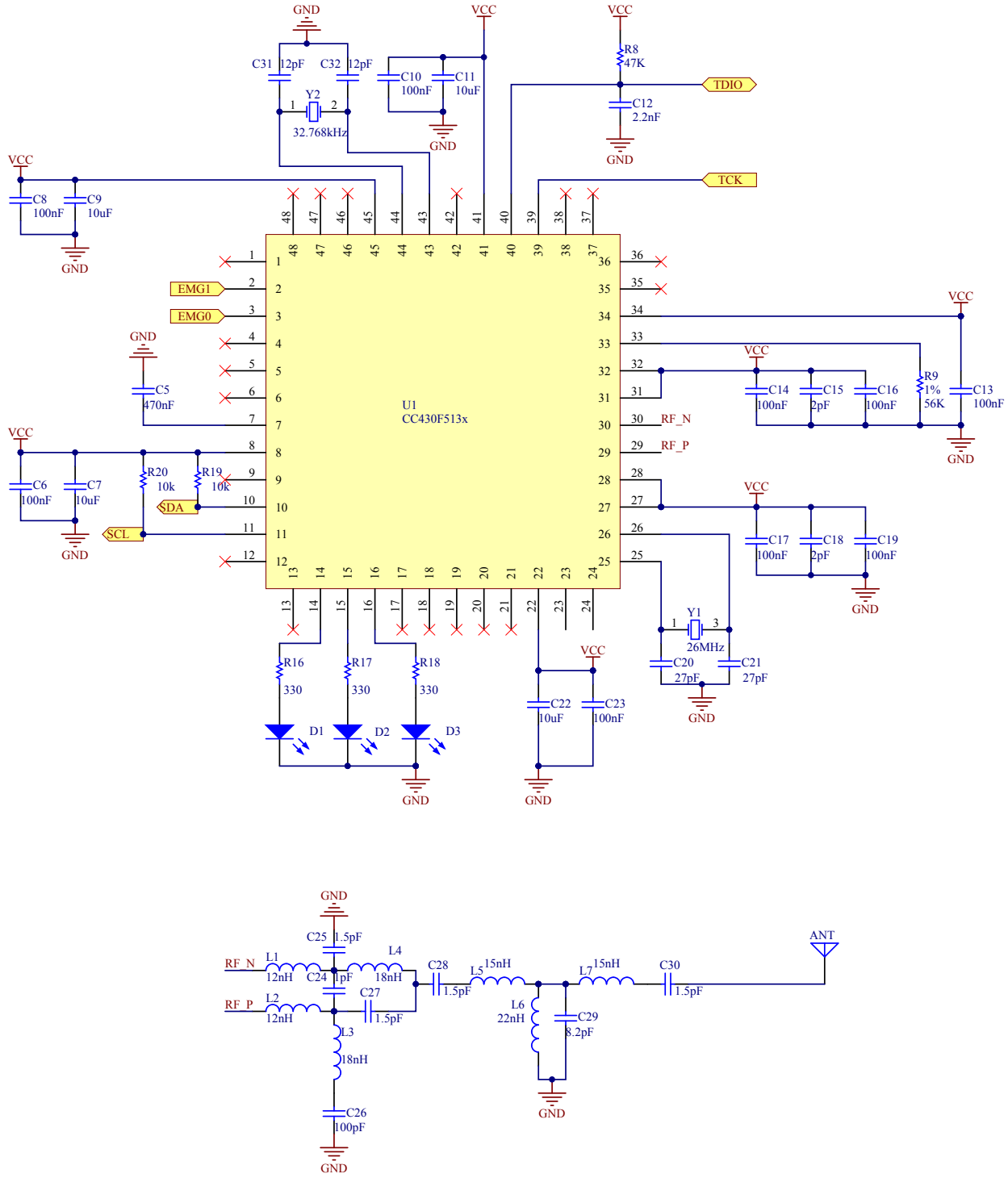

Figure 2.4: Subschematic of the 2 channel wireless EMG system PCB showing the details of the CC430 IC's implementation on-board.

2.1.2 Results

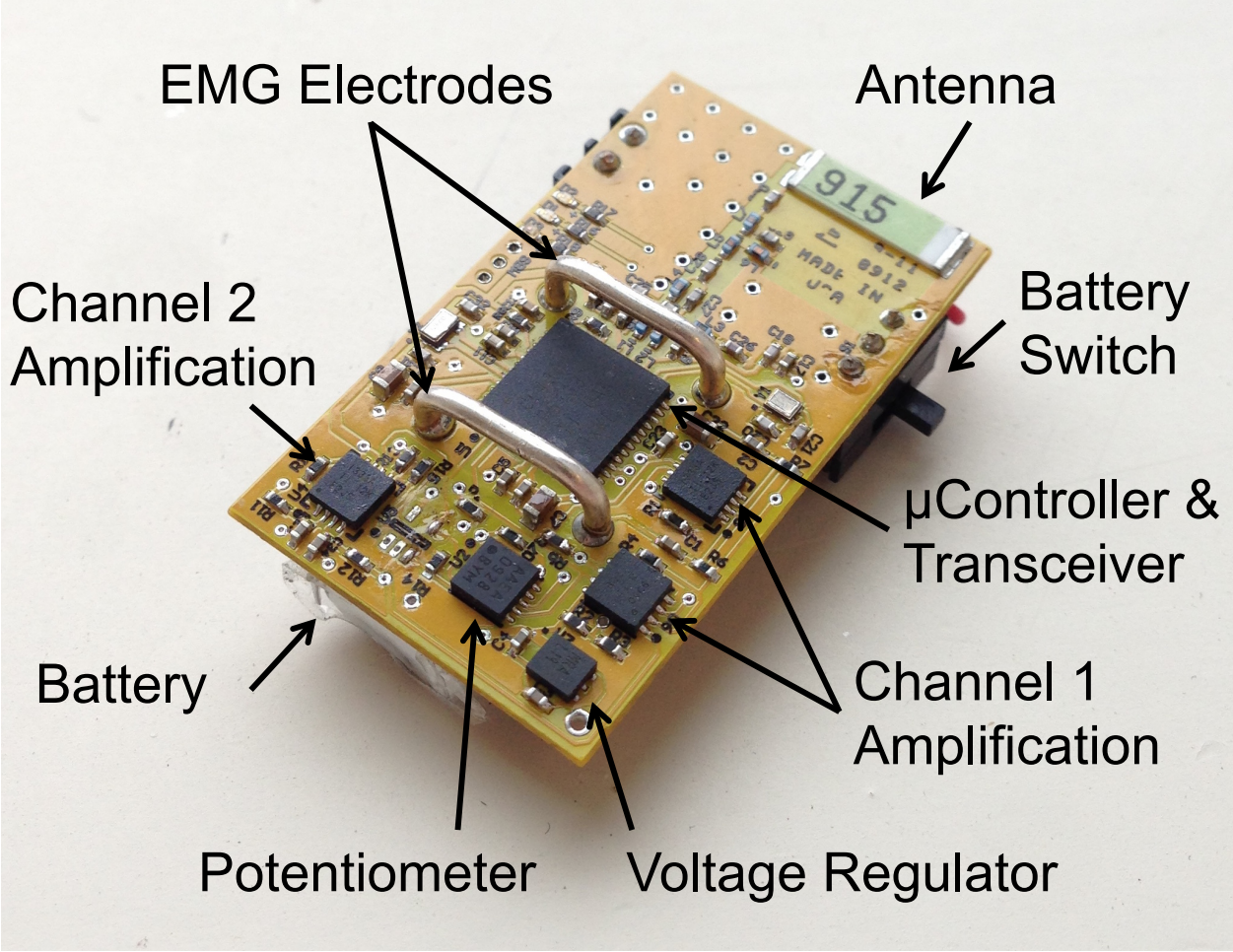

Figure 2.5: Assembled wireless EMG sensor. Note this device does not have the 2nd state amplifier populated for channel 2 as the particular application did not require additional gain after the IA on this channel. The IA signal in this channel is directly passed to the ADC via the potentiometer.

The EMG sensor (shown in Figure 2.5) measures 2.2 x 3.7 x 0.75 cm^3. On the top side (visible) are all of the electronics (microcontroller, amplifiers, passive components, etc.). On the back is a 3.0 V, 500 mAh rechargeable lithium-ion battery and a switch to turn the device on and off. Each printed circuit board (PCB) has pads for the entire electronics package

for 2 EMG sensors but only space for a single channel of EMG electrodes. By design the second channel is intended for a different physical location on the human body from the first channel. To achieve this physical separation a second PCB is populated only with EMG electrodes and then wired to the electronics package contained on the first channel's PCB. Figure 2.6 shows recorded EMG data from the device. In this example the user was alternating between extending the wrist angle (extensor muscles activated) and contracting the wrist (flexor muscles activated).

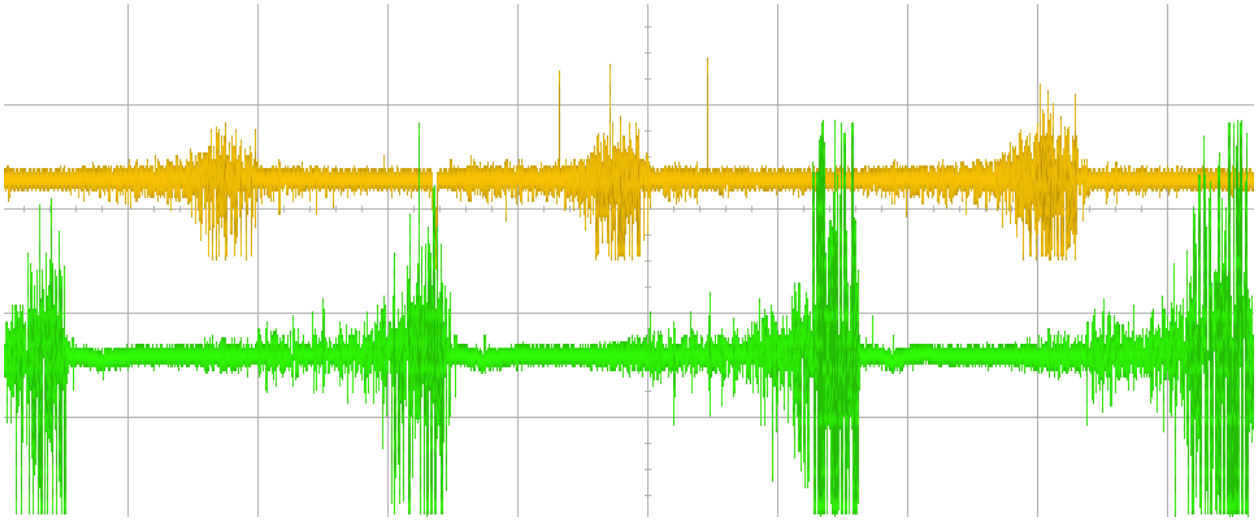

Figure 2.6: 2 channels of wirelessly received EMG data from a human subject. Channel 1 (yellow) shows EMG activity of the extensor muscle group, channel 2 (green) is flexor EMG.

The CC430 has a maximum data rate of 500 kbps which means the system can transmit data much faster than the EMG data streams require. Instead of running at a slower data rate the EMG system designed here uses the maximum data rate and disables the transceiver when no data packet is ready for transmission. This duty-cycling of the transmitter results in an approximately 50% power savings. Figure 2.7 shows the power profile of the device going through two packet transmission periods. Total power consumption of the 2-channel EMG sensing device is approximately 35 mW from a nominal 3.0 V source giving a total lifetime before recharge of just over 14 hours of continuous EMG sampling and wireless transmission.

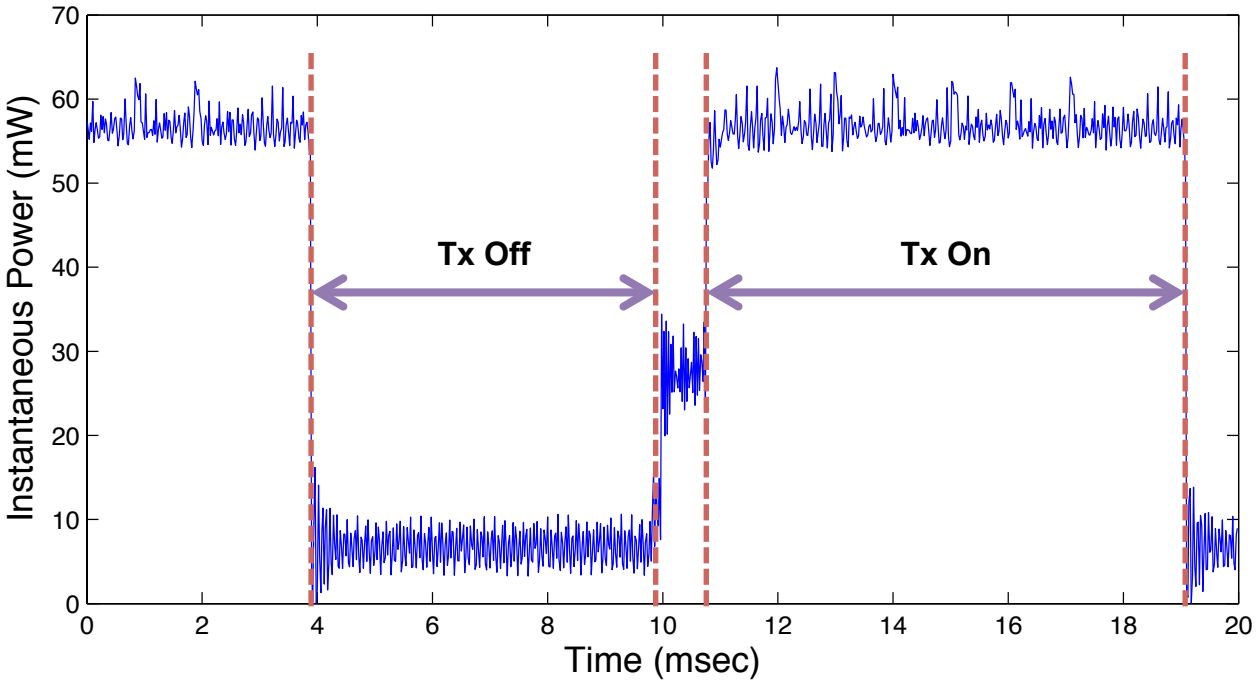

Figure 2.7: Instantaneous power profile of an active EMG sensor.

2.1.3 Conclusion

The design shown above is a fully self-contained wireless 2-channel EMG system suitable for human usage. Signal amplification allows for clear reading of EMG activity without the need for wires to connect the patient to a wired amplification setup. Allowing variable gain also makes this design suitable for many other EMG applications as EMG signals can be weaker or stronger depending on orientation and which muscle groups are targeted.

Battery lifetime of the device is well over a normal day's use in a clinical setting thanks to the large battery pack included with the sensor package. Unfortunately this large battery dictates the overall size of the device. While acceptable in a clinical setting where patients are trained to expect uncomfortable/bulky sensors the size is too large for wide-spread at-home usage among the general populace. Moving forward it is clear that the EMG system's design must be changed to reduce overall power consumption significantly to enable a smaller form factor.

2.2 'Neurogame Therapy' for Improvement of Movement Coordination after Brain Injury: Developing a Wireless Biosignal Game Therapy System [1]

Emerging technology holds tremendous promise for improving recovery following brain injury. Here we describe a home-based rehabilitation system for improving volitional control of hand movement. People with cerebral palsy and those recovering from stroke or traumatic brain injury often have difficulty producing coordinated movements of the hand and arm on one side of the body. Surface electromyography (sEMG) recorded over affected muscles is used to provide enhanced visual feedback via a computer game interface. Several weeks of practice using this system has resulted in improved muscle coordination. Preliminary results are shown from the next generation of this system, which will employ ultra-low power wireless sensors to transmit muscle activity to a home computer.

2.2.1 Introdution

Persons with cerebral palsy and those recovering from traumatic brain injury or stroke often experience reduced motor control. In the case of hand and arm motion, movement impairment can substantially disrupt daily activities and dramatically reduce quality of life. Two impairments that are common to all three groups are hemiparesis and spasticity. Hemiparesis is decreased motor control with secondary weakness that occurs on one side of the body, typically the side opposite the brain injury. Spasticity is characterized by over-active muscles, and is common after stroke and incomplete spinal injury, as well as for those with cerebral palsy [2]. Over half of persons after stroke exhibit some form of pathologic muscle tone well into the chronic phase [3]. Hemiparesis and spasticity make it difficult for persons to use their impaired upper extremity in daily tasks [4], [5].

Although disabilities can be severe, these individuals can substantially improve motor function with large amounts of physical therapy and repetitive practice at specific tasks [6]-[8]. Neural plasticity studies suggest that with adequate practice of key activities, where the individual is motivated and the demands on the nervous system are gradually increased,

permanent improvements in motor control can occur [9]-[12]. Current clinical therapy regimens that are covered by insurance, however, cannot provide enough practice time to affect maximum recovery, and adherence to home exercise programs is generally poor.

2.2.2 Neurogame Therapy Concept

Here we demonstrate a method to overcome the limitations of in-clinic practice time and home exercise motivation by providing an effective, enjoyable and flexible home therapy solution. The final system will use wireless surface electromyography (sEMG) recorded from the skin over impaired muscle groups to control the movements of existing computer games (Figure 2.8).

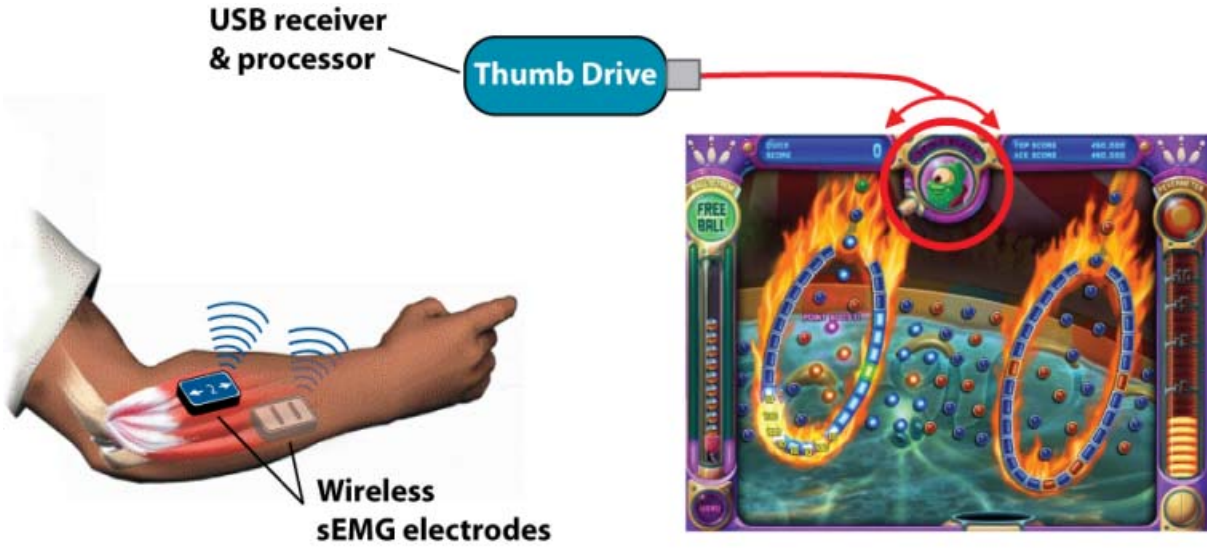

Figure 2.8: Schematic of the Neurogame therapy system where surface muscle electrical activity (sEMG) is converted to movements of popular computer games via wireless electrodes interfacing with a USB thumb drive receiver.

Using this approach, any muscle or muscle group in need of improved volitional control can be used to control game movements in patterns chosen for therapy. Muscle-driven movements of the game provide enhanced visual feedback of neural activity, including weak muscle

activity that does not cause overt movements. A similar approach of using surface EMG to control computer mouse movements has been used in the clinic for the lower extremity with great success in retraining gait for individuals with hemiplegia following brain injury [13], [14].

Using a flexible transform from muscle activity to game control permits reinforcement of either increased or decreased activity (e.g., reduced spasticity) for each muscle, as well as coordination of multiple muscles into functional synergies.

The proven psychological reward schedule of popular computer games provides ample motivation to practice the desired muscle patterns, and even older adults enjoy computer games [15], [16]. Neurogame therapy users improve muscular coordination gradually by working through the incrementing difficulty levels of the game, as well as through tuning of the transform converting muscle activity to game control.

Advantages over existing game rehabilitation methods

Using muscle activity directly to control computer games has several advantages over exiting methods of game-based rehabilitation [17], [18], including the use of virtual reality [19] or acceleration-sensing controllers like the Nintendo Wii [20]. The direct use of muscle electrical activity provides a more flexible control signal compared to overt movements of the limbs needed to register a force or acceleration of existing game controllers. For example, weakly activated muscles often produce detectable EMG signals without causing movements of the limb. Our approach amplifies these weak signals into enhanced visual feedback, while gradually increasing the magnitude of this activity through incrementing difficulty levels. In addition, many daily tasks do not require limb movements, but rather co-contraction of functional muscle synergies to stabilize a joint in a desired posture. Our method permits these functional muscle synergies to be selectively reinforced through the game environment, with the goal of improving activity and participation in life skills.

Direct feedback of muscle activity also permits training of accessory muscles that may be inhibiting movement. For example, muscles throughout the upper extremity are frequently

spastic in children with cerebral palsy, leading to a flexed posture of the arm [4], [6]. This flexible approach could gradually reinforce children for relaxing these overactive muscles in order to control the game, leading to more natural movements of the entire extremity. A significant advantage of the Neurogame therapy approach is the ability to target the most impaired muscles throughout the body, and provide customized visual feedback for each user in order to improve his/her muscle coordination.

2.2.3 Wireless Neurogame System

Recording sEMG signals requires a bipolar electrode placed directly on the surface of the skin. It is desirable to make the recording electronics and electrodes as small and unobtrusive as possible. To that end, wireless connectivity between the sensor and the computer is critical. The following system-level requirements were considered:

- sEMG signals are on the order of mV with a bandwidth of interest from roughly 10 Hz-1 kHz.
- The wireless electrode must perform amplification and digitization.
- An 8-bit ADC is demonstrated as being sufficient for Neurogame therapy.
- A low power custom IC would have a supply voltage of roughly 1V. Thus, the on-chip amplifier should have a programmable gain with a maximum of at least 60 dB and a noise floor less than 100 Vrms.
- Data must be continuously streamed at a rate of roughly 8bit * 3 ksps = 24 kbps.
- Small form-factor and weight (less than a few grams). Thus, a small hearing aid battery or rechargeable LiPo battery should be used.

Table 2.1: Comparison of Wireless EMG Sensors

	Battery Life	Weight (grams)	Freq (GHz)	Sample Rate	Range(m)
BTS FreeEMG	5 h	9	2.4	4 kHz	50
ZeroWire	8 h	12	2.4	2 kHz	20
TeleMyo	8 h	14	2.4	3 kHz	10
Proposed	>70 h	1	0.4	3 kHz	10

- The power consumption must be minimized since a small battery is desirable. A 30mAh hearing aid battery, for example, would require an overall system current less than 5mA for a reasonable battery life.

Low noise amplifier ICs, ADCs, and microcontrollers that comfortably meet these specifications can be readily purchased. However, commercially-available RF transceiver technology is notoriously power hungry. Low power 2.4 GHz Zigbee radios, for example, dissipate over 20mW while transmitting and receiving. Thus, we conclude that the most challenging part of the system design will be the RF transceiver. This observation is reinforced by a review of commercially-available wireless EMG systems (see Table 2.1).

We have designed a customized IC that integrates all functions necessary for wireless EMG recording (programmable amplification, ADC, digital logic, 400 MHz transmitter). As shown in Table 2.1, we achieve a significant reduction in weight as well as a large increase in battery life. Much of this improvement comes from the huge reduction in power consumption achieved by our RF transmitter design. This section will describe this system in detail.

Integrated Circuit Design

Our objective with this chip design was a single-chip wireless sensor for sEMG and other bio-signals. The chip architecture is shown in Figure 2.9 below [21].

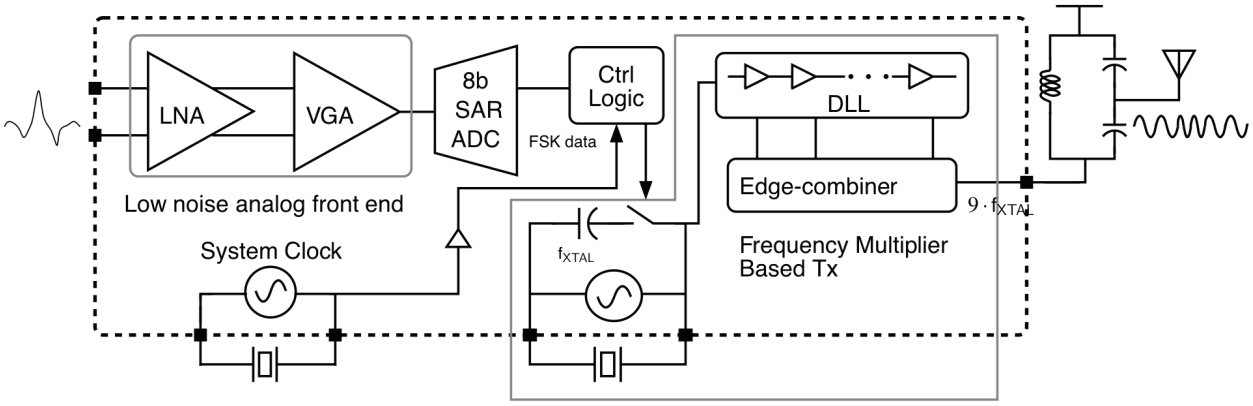

Figure 2.9: Architecture of the wireless EMG chip.

The chip has a fully-differential low noise input (noise floor of 3 μVrms, programmable gain up to 80 dB, and bandwidth of 7 kHz). This front-end exceeds the specifications for sEMG recording by a large margin and dissipates less than 20 μW. An on-chip 8-bit successive-approximation ADC is integrated and allows a variable sample rate. A 400 MHz frequency-multiplying transmitter was used. This architecture allows extremely low levels of power dissipation (less than 0.5 mW) and can be configured to operate in multiple frequency bands (e.g. 405 MHz MICS or 433 MHz ISM bands). We have since published subsequent versions of this transmitter and an accompanying receiver [22]-[24].

This chip was fabricated in a 0.13 μm CMOS process. The die photo is shown below in Figure 2.10. The entire chip dissipates 500 μW when transmitting continuous EMG data. This represents a significant reduction in power dissipation and size compared to solutions using commercially-available ICs.

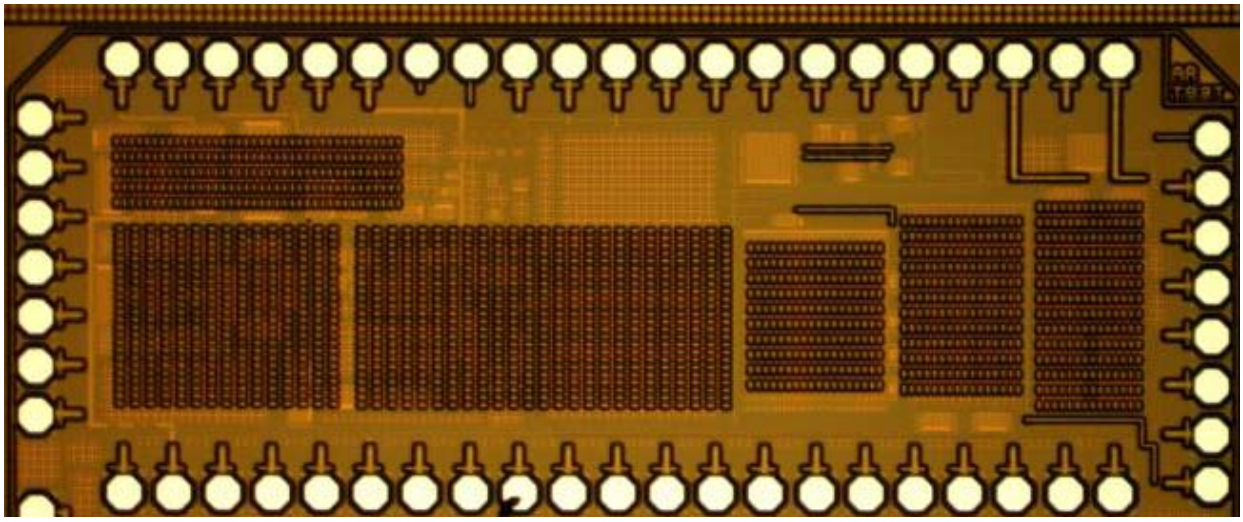

Figure 2.10: Wireless sEMG die photo (1mm x 2.5 mm^2).

Board and electrode design

All circuitry is integrated onto a single chip, so the final product can be extremely small since minimal support circuitry is required. The system uses a thin 4-layer PCB measuring only 7.6 x 8.7 mm^2 which incorporates the single chip, two quartz reference crystals, a voltage regulator and matching circuitry to interface the chip to an attached antenna. The fully-populated PCB weighs 0.18 g without battery, 0.3 g with a 337 battery, and 0.34g with a size 5 zinc-air battery. The deployed board used epoxy encapsulation to protect the bondwires.

A simple enclosure (seen in Figure 2.13) was developed to house this PCB, leaving only two electrodes outside the case for direct skin contact for sensing EMG signals. The case itself was created using Computer Aided Drafting (CAD) software and a rapid prototyping machine, which takes the digital design from the CAD software and directly creates a plastic part. The electrodes are comprised of silver wires, which provide good electrical contact to the skin and are easily solderable, facilitating connection to the electronics.

Receiver design

An inexpensive receiver system was designed to collect the data transmitted from the EMG tag. The block diagram for the receiver is shown in Figure 2.11. This receiver demodulates the incoming RF signal from the tag, decodes the received packet and outputs the raw EMG data, both digitally via USB as well as outputting a pure analog waveform for use with analog sensing equipment such as an oscilloscope.

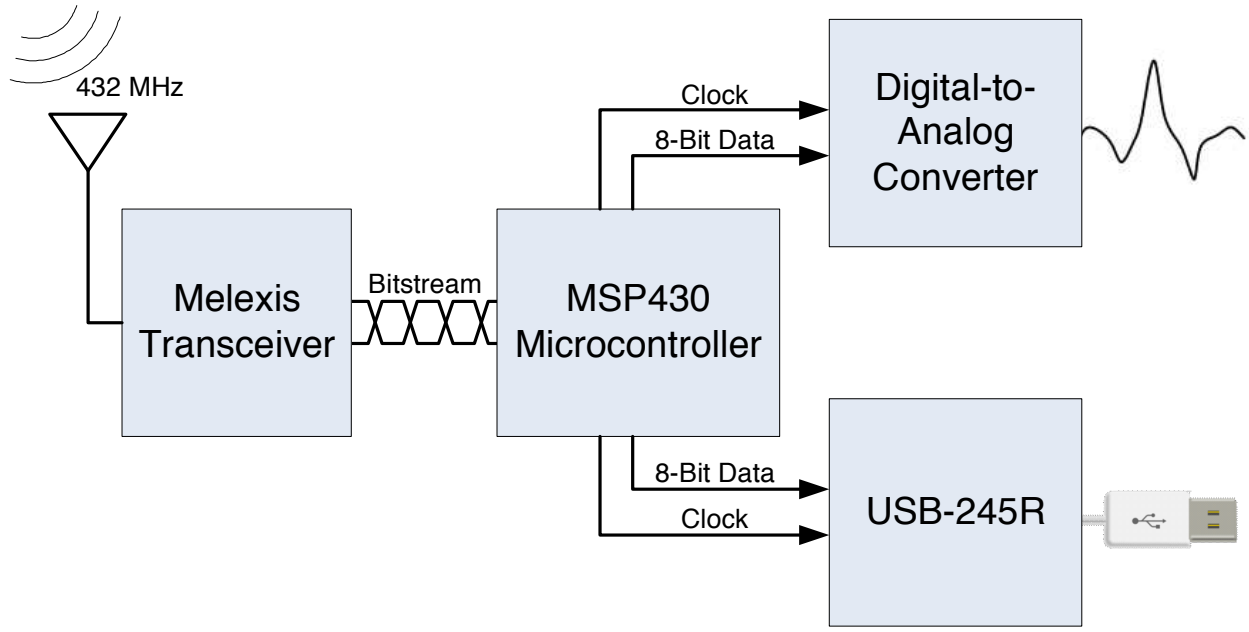

Figure 2.11: Companion receiver block diagram.

Demodulation occurs within the SiLabs 4320 receiver. The resulting baseband bitstream is processed by a Texas Instruments MSP430 microcontroller, which runs a custom clock and data recovery (CDR) algorithm to determine the 1s and 0s of the bitstream.

The tag transmits a 011 binary pattern before each packet of data; our CDR takes advantage of this guaranteed 0-to-1 transition before a packet by re-syncing the receivers timing to the transmitter by using this time as a known point (effectively zeroing out the Rx clock). This makes the receiver quite tolerant to variances between the Tx and Rx clocks.

An extreme example of Tx/Rx clock mismatch is shown below in Figure 2.12. Here we see that the microcontroller waits a given amount of time, determined by its internal clock, to sample the bitstream and determine the value of each bit. If this internal microcontroller clock does not match perfectly with the clock used by the transmitter, the sampling train of the microcontroller will appear to drift away from the center of each bit, eventually resulting in either skipping a bit entirely (clock too slow) or reading a single bit twice (clock too fast). To avoid this potential problem the microcontroller re-syncs its sampling train during the 0-1 transition contained in the header pattern by scheduling the next sample to take place one half of a bit period after this transition, instead of a full bit period after the previous sample as is done every other time. Theoretically, this method can tolerate as much as a 4.5% mismatch in clocks (maximum drift of 50% of a bit period over eleven total bits per packet).

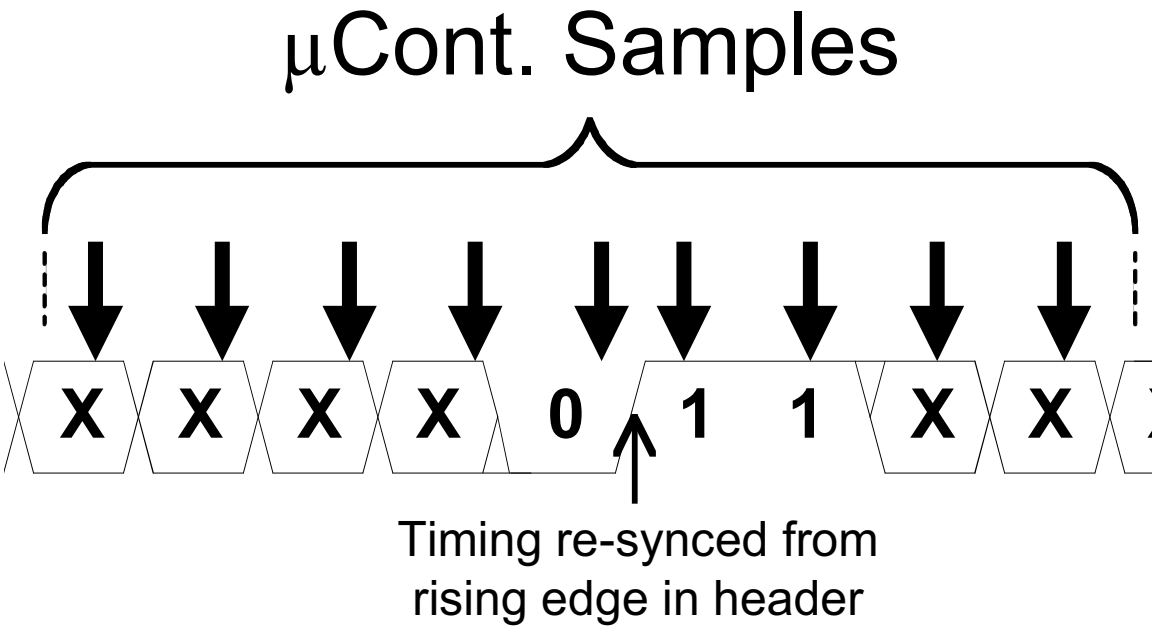

Figure 2.12: Rx timing synchronization with frequency mismatch.

The final extracted data is then sent digitally via USB (using FTDIs FT245R chip) to

a PC. In addition, there is a digital-to-analog converter onboard the receiver that outputs a reconstructed analog signal. This CDR algorithm is run on the fly, allowing real-time reconstruction of the analog waveform for viewing on a scope or for audio playback. The entire receiver system is powered by USB from the 5 V bus connection.

Based on the custom IC described in the previous section, we have developed miniaturized wireless EMG electrodes. This circuit measures less than 1 cm^2 and fits easily in the electrode casing shown in Figure 2.13. We used this device to record activity from a forearm muscle and transmit the signal five meters to the USB-compatible receiver (Figure 2.2.3).

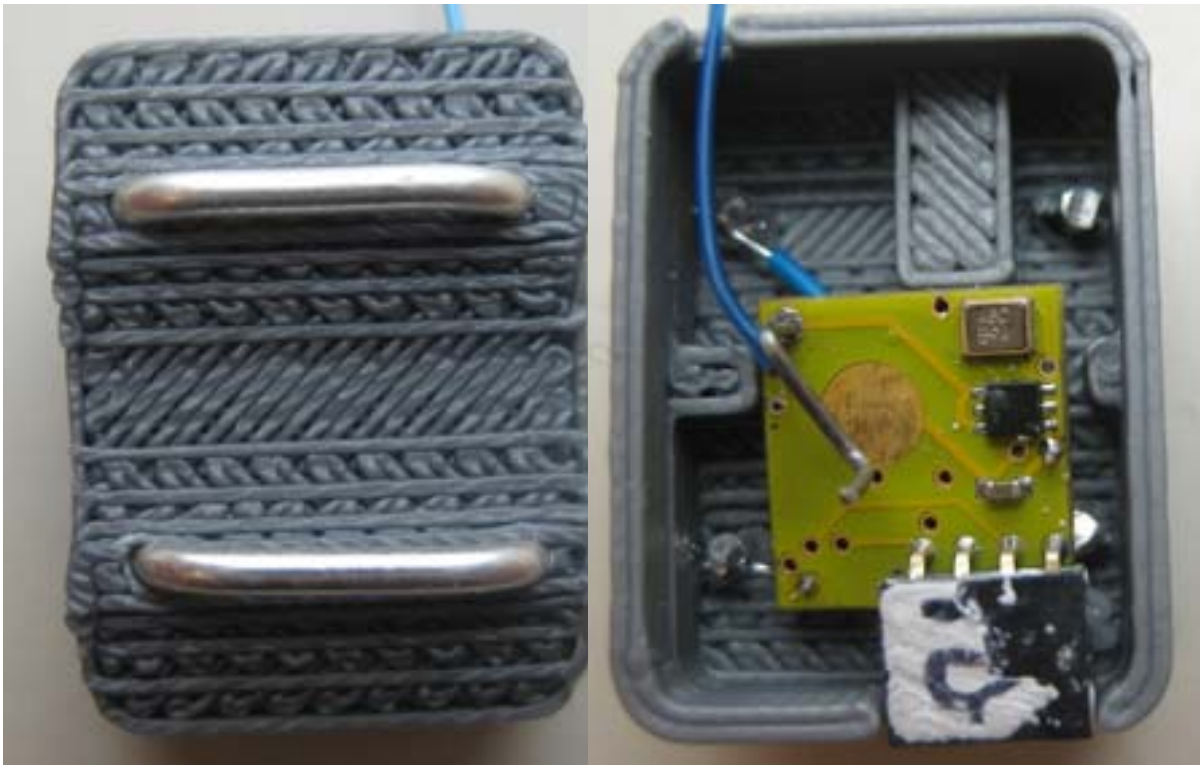

Figure 2.13a: Prototype electrode casing, showing the electrodes (left) and wireless transmitter circuit inside (right).

Figure 2.14 shows the functional block diagram of an early prototype of the wEMG system. The entire system is powered from a single 0.13 g coin-cell battery, which is subse-

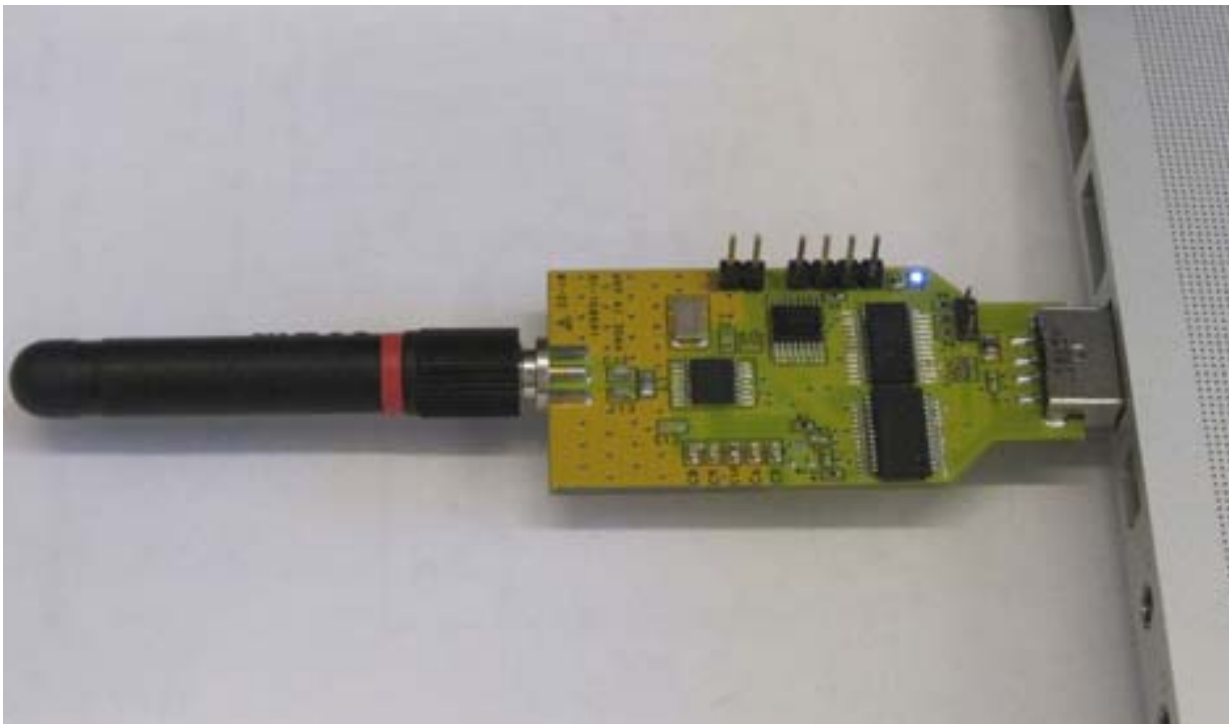

Figure 2.13b: Functioning receiver board with USB output to a computer.

quently regulated to 1 V. Other than this regulator IC, all functionality is performed by the custom-designed IC.

Our initial deployment of the board is as a low power, unobtrusive EMG sensor. Differential EMG probes were used to record muscle activity for Neurogame therapy. The probes were attached to the skin over forearm muscles. The signal was transmitted over 10 meters to our USB-compatible receiver. Figure 2.15 (right) shows the reconstructed waveform resulting from three muscle contractions.

2.2.4 Evidence for Improved Muscle Coordination

Two children with cerebral palsy and two adults, one with traumatic brain injury (TBI) and one with stroke, have successfully used an early prototype of the Neurogame therapy system both in the clinic and at home. Muscle activity recorded from their affected wrist

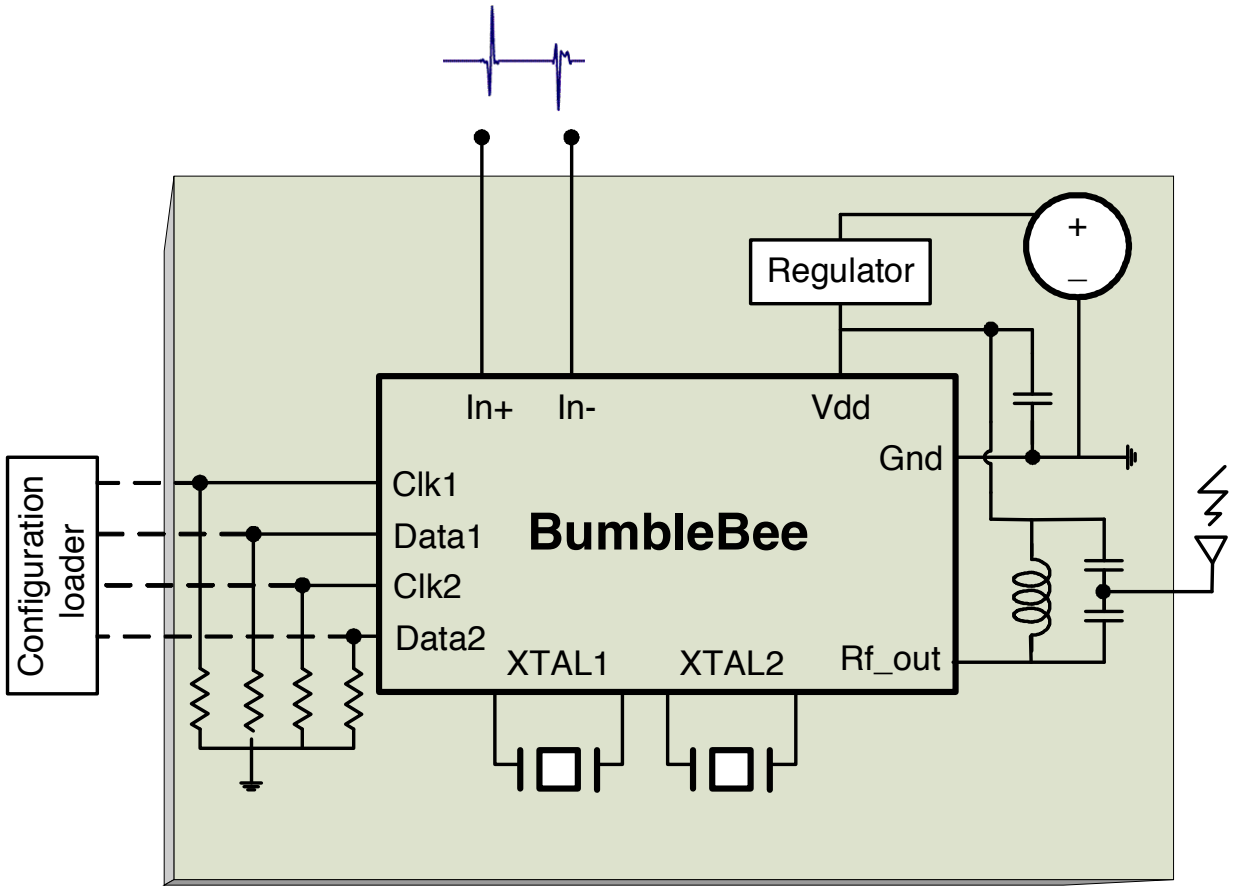

Figure 2.14a: Wireless sEMG datasheet block diagram.

flexor and extensor muscles controlled the game system for 30 minutes/session occurring 3-5 times/week over 4-5 weeks. The total number of game sessions ranged from 15-30. All subjects improved muscle coordination as a result of game training.

Improved range of motion

The first subject with cerebral palsy improved active range of motion substantially after playing the game. This was evident in his ability to extend his wrist (Figure 2.16). Before game training, this child could not extend his wrist beyond approximately 92°(Figure 2.16 left). After 15 days of game practice, he could extend his wrist to 170°(Figure 2.16 right).

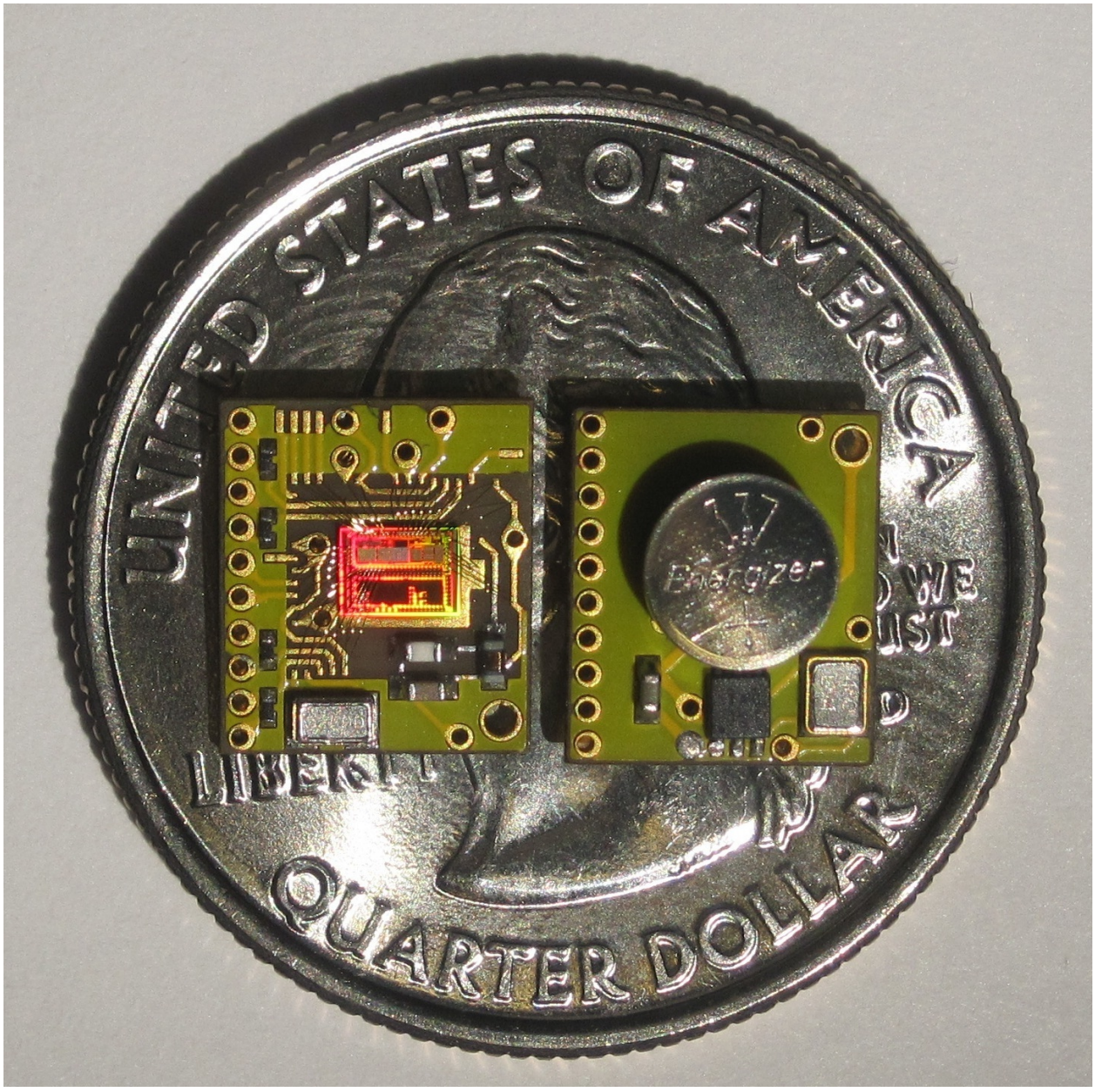

Figure 2.14b: Front and back of the PCB. A thin 30 gauge wire-wrap monopole wire antenna a few cm long allows >10 m range.

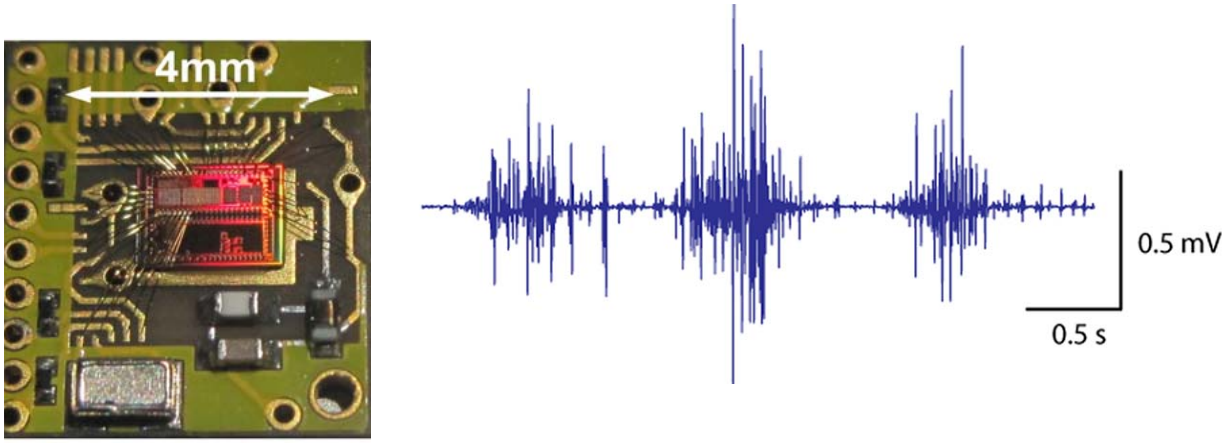

Figure 2.15: A miniature wireless EMG circuit (left) capable of amplifying, filtering, digitizing and transmitting bi-polar EMG signals (right).

This improvement was maintained for over three months with no further therapy.

Volitional control of paretic extensor muscles

Both of our adult subjects dramatically improved their ability to activate weak and paretic extensor muscles as a result of game training. Figure 2.17 shows the 3.5-fold improvement in muscle activity demonstrated by adult subject #3 with traumatic brain injury over the one-month game training period. This improvement is especially notable given that this subject was in the chronic phase of recovery, 4 years after injury. The fourth subject recovering from stroke also improved extensor muscle activation by nearly 4-fold during her period of game training.

Independent muscle activity

All subjects dramatically improved their ability to independently activate antagonist muscle groups. Before game training, no subject could activate wrist flexors and extensors independently more than 20-40% of the time (2.18). After game practice, all subjects could consistently achieve 60-90% independent muscle control.

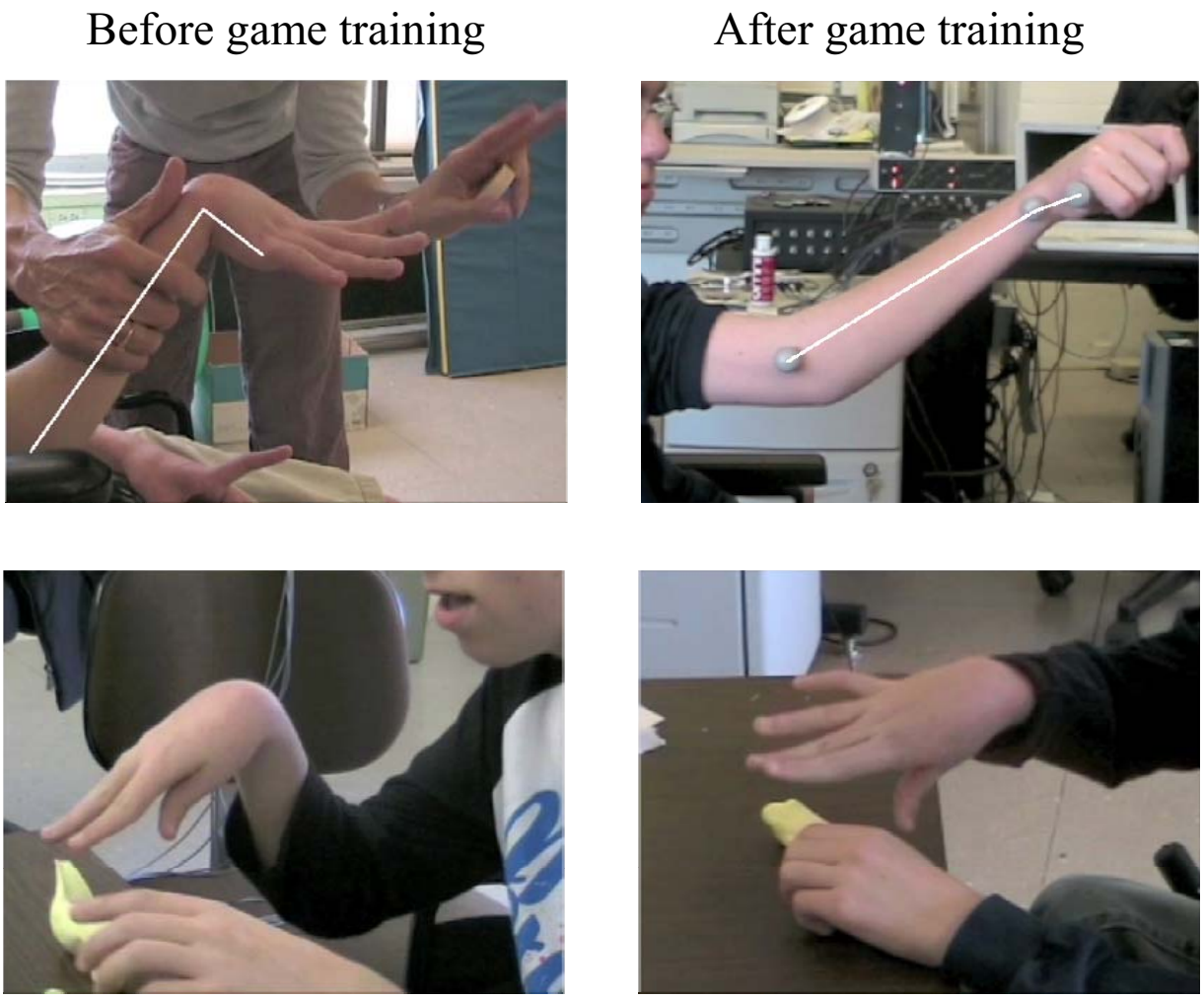

Figure 2.16: Wrist movements for subject with cerebral palsy before (left) and after (Right) game play for only 15 sessions. White lines indicate angle of maximum wrist extension within the sagittal plane (top row). Bottom row shows the subject spontaneously adopting a more extended wrist posture during functional testing.

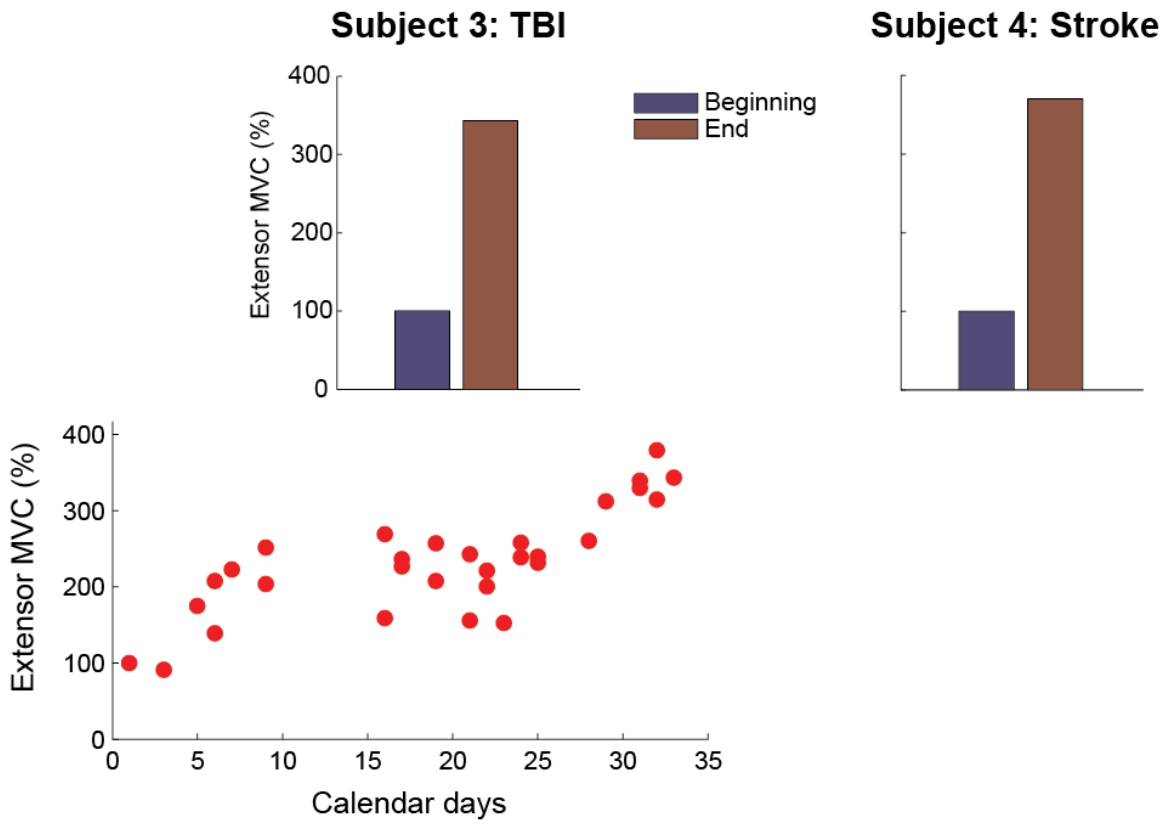

Figure 2.17: Maximal extensor muscle EMG for an adult with TBI increased by nearly 4-fold with 1 month of game training.

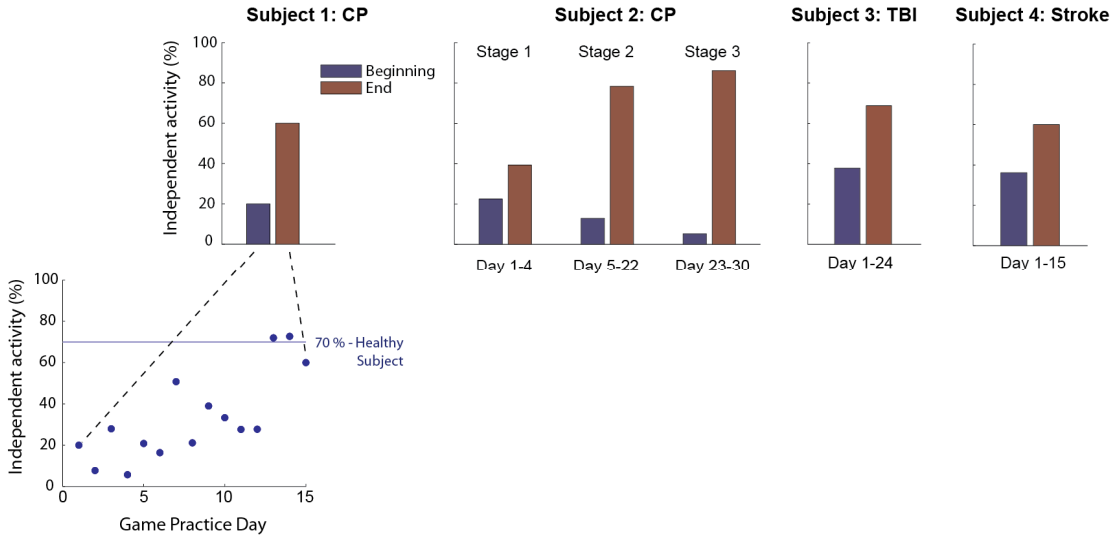

Figure 2.18: Independent muscle activity for two children with cerebral palsy (CP), one adult with traumatic brain injury (TBI), and one adult recovering from stroke. Bar graphs show independence at the beginning and end of each stage of game training. All subjects improved independence to near the level of a healthy subject (horizontal line at 70%).

Bar graphs in Figure 2.18 show independence at the beginning and end of each stage of game training. Prolonged game training for Subject 2 permitted the game to be adjusted in several stages of difficulty, each requiring progressively more independent muscle control. All subjects improved their independence to nearly the level of a healthy subject indicated by the horizontal line at 70%.

All subjects performed the game therapy at home as much or more than requested (3-5 days/week). They also rated the game therapy very highly for both enjoyment and for its positive effect on their hand function in general activities.

2.2.5 Conclusion

This flexible and enjoyable method of retraining muscle activity for functional movements has the potential to substantially impact the treatment of brain injury and other movement disabilities. Prolonged practice with visual feedback of specific patterns of muscle activity under strongly motivating conditions likely leads to long-term changes in the strength of neural connections within the motor system. Further prototype development will potentially lead to a low- cost version of Neurogame therapy that could be made affordable enough for individuals to purchase (even without insurance coverage). Thus, this intervention could prove an affordable and effective method for retraining the brain to produce coordinated movements after injury.

2.2.6 Acknowledgements

The authors thank Larry Shupe, Bob Price and John Burt for expert programming assistance, Anat Lubetzky-Vilnai, Elena Donoso-Brown and Karli Gutman for valuable assistance in data collection and analysis, Kevin Flick for insightful discussions, Dan Landeck and PopCap Games for enthusiastic support, Spencer Gibbs and Luis Perez for the electrode enclosure fabrication and electrode battery charger design, and the Wireless Sensing Lab team for the custom IC design.

Chapter 3

A 0.5 CM^3 FOUR-CHANNEL 1.1 MW WIRELESS BIOSIGNAL INTERFACE WITH 20 M RANGE [25]

Chapter 3 presents a self-contained, single-chip biosignal monitoring system with wireless programmability and telemetry interface suitable for mainstream healthcare applications. The system consists of low-noise front end amplifiers, ADC, MICS/ISM transmitter and infrared programming capability to configure the state of the chip. An on-chip packetizer ensures easy pairing with standard off-the-shelf receivers. The chip is realized in the IBM 130 nm CMOS process with an area of 2x2 mm^2. The entire system consumes 1.07 mW from a 1.2 V supply. It weighs 0.6 g including a zinc-air battery. The system has been extensively tested in *in vivo* biological experiments and requires minimal human interaction or calibration.

3.1 Introduction

There is a tremendous emerging need for small, wireless, high-performance biosignal monitoring devices. There are existing devices that are currently deployed in relatively small numbers in animal research laboratories and serving as chronic implants. Researchers are also working on devices for clinical use and specialty athletic purposes. However, there are still barriers preventing widespread deployment of wireless devices in mainstream medical monitoring. Each application has specific challenges unique to its implementation, for example motion artifacts in body worn electrocardiograph (ECG) sensors and 60 Hz interference overriding low-level signal recordings. Each challenge can be addressed with a hardware approach on the device, but such a device becomes more application specific with these additions. The approach presented here takes a different view, preferring to create a device

that is useful in a wide swath of applications, dealing with many of these application specific problems with either device programmability or digital signal conditioning off-chip. In this way we can develop a device that while it may not address each applications issues ideally, is useful for a wide range of diverse applications.

Our specification development was guided by the desire to have a device that worked over ECG, EMG, and spike-based neural recording paradigms. To define the needed technical requirements, two distinctly different applications were chosen that bookend the envisioned range of uses this device will be well suited for: human ECG and small animal (such as a mouse) extracellular single unit neuron recording. Human ECG exhibits fairly large voltage amplitudes (mVs) and low frequency content (150 Hz minimum). Single unit neuron recording voltage amplitudes can vary widely, from 10s of μVs to mVs depending on electrode placement and low frequency potentials (LFP). Frequency content here is much higher (over 1 kHz). While device weight is not a realistic limiting factor for a human, the device should be small enough and have a long enough wireless range to allow the subject freedom of movement. Conversely, weight and size are key constraints for applications on small animals such as a mouse. The device must be small enough for the animal to conformably carry without affecting its normal behavior. Both uses would benefit from a long lifetime running from a single battery; while in the ECG case its reasonable to extend the lifetime with a larger battery the small animal case requires a low-power design to maximize lifetime from a small battery due to the size constraint.

The main challenge lies in integrating the entire system in a small form factor of <1 cm^3, with a weight of <1 g and low-power consumption (<10 mW) making them suitable for mass deployment. The signal chain in the system should have low input referred noise (a few μVrms) and sufficient dynamic range to accommodate the recording of different signal modalities (single unit recording, electrocardiography (ECG), electromyography (EMG)). Depending on the recording site location and condition the biosignal amplitude can vary widely, thus the gain and bandwidth of the amplifier front-end should be programmable on-the-fly to compensate. The monitoring device should also suppress motion artifacts to

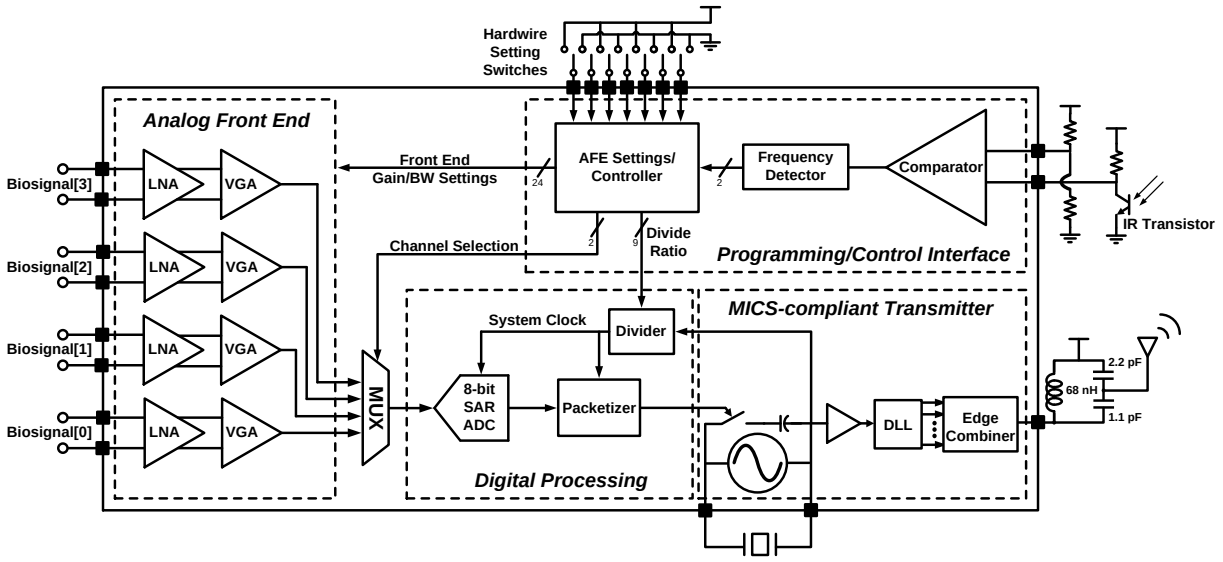

Figure 3.1: Block diagram of the wireless biosignal monitor.

achieve long term portable biosignal monitoring. Lastly, the device needs to have a reliable, low-power communication interface to transmit the digitized biosignal to an external receiver. This necessitates the integration of a low-power transmitter that is capable of communicating reliably within an existing wireless infrastructure.

There has been a lot of recent effort to meet the above challenges. The configurability of the front-end depending on the recording mode and site requires closed-loop communication between the sensor node and the outside world. The wireless programming scheme should be simple enough to be used by scientists and clinicians with little electronics background. Previous biosignal monitoring devices such as [26][27][28][29][30] fail to provide simple low power wireless configurability. Artifacts in recorded biosignals are common due to motion, bioelectrical activity, etc. If not mitigated these corrupting artifacts can seriously degrade the quality of recorded signal. Many techniques have been developed to combat these artifacts, for example the suppression of motion artifacts in the analog domain has been recently explored for ECG monitoring systems [31]. However, instead of implementing signal conditioning circuitry on-chip the system presented here post processes the digital signals from

high dynamic range readout circuitry to tackle the problem of motion and other artifacts without biosignal specific circuitry, keeping the amplifier inputs more biosignal source agnostic.

The wireless telemetry of the digitized biosignals requires a low-power transmitter to establish a robust communication link with a basestation. The requirements of a wireless transmitter for a biosignal monitoring device include low power consumption, stable frequency generation, fast start-up time and compatibility with relevant frequency bands. The telemetry link could be established using an inductive link [32] or through RF communication. The range of inductive links is limited. Ultrawideband (UWB) is an attractive option, particularly for massively parallel multichannel systems where the data rate requirements are high [30]. However, this requires complex synchronization [33] and is susceptible to jamming due to the wide-open receiver RF front-end. Low power open-loop transmitters [29] experience drift as they are not locked to any reference signal using a crystal and hence their use in mainstream healthcare devices that require manufacturability and high yield/reliability is difficult. Therefore, a narrowband transmitter with a stable frequency generation scheme and low power consumption is a prudent choice for a wireless biosignal monitoring device.

Even though some of the challenges have been met individually, previous biosignal monitoring devices such as [26][27][28][29][34] fail to achieve all of the stated objectives in a single system. This work represents the third generation of a single-chip system that allows robust wireless biosignal monitoring. Our goal is to describe decisions made in the design of the IC that allowed a low overall power dissipation and form-factor when deployed in actual monitoring environments. The chapter is organized as follows. Section 3.2 outlines the system description with a focus on the Programming/Control Interface, the Analog Front End (AFE), the Analog-Transmitter Interface and the MICS compliant transmitter. Section 3.3 presents the measured results on the laboratory bench, *in vivo* experiments with mice and ECG monitoring of a human. Section 3.4 summarizes the main design decisions and results.

Table 3.1: Chip actions based on the IR signal detected

Frequency Detected	**Chip characteristic changed**
36 kHz	Select next channel for transmission
38 kHz	Increment gain setting
40 kHz	Increment high pass cut-off frequency setting

3.2 System Description

The overall architecture of the four channel biosignal monitor is shown in Fig. 3.1. The analog front-end comprises four low-noise, fully differential amplifiers designed to interface directly with electrodes connected to tissue, followed by a variable gain amplifier to accommodate different signal modalities. One amplified channel is selected and digitized using an on-chip 8-bit successive approximation register (SAR) ADC. The digitized data is buffered, appended with a programmable header, and tagged with cyclical redundancy check (CRC) information to detect communication errors. Finally, the digital bits are transmitted using a sub-mW frequency-multiplying transmitter. A programmable system clock is derived from the radio's 48 MHz crystal reference. To enable on-the-fly programming of the chip, an infrared (IR) phototransistor interface is integrated into the system. The IR interface, tuned to 935 nm, allows wireless programming of the gain/bandwidth settings of each variable gain amplifier (VGA) independently and selects the active channel for transmission. All of these settings changes can be made on-the-fly using an infrared programmer to fine-tune the device for optimal recording during use.

3.2.1 Programming/Control Interface

A biosignal monitor often requires on-the-fly changes in gain and bandwidth to accommodate different recording site conditions and provide the ability to switch channels to target specific

electrodes. A continuously running RF receiver would dissipate a significant amount of power, we instead propose a low power ($< 1\,\mu$W) wireless infrared interface using an off-chip IR phototransistor sensitive to 935 nm wavelength light. The incident IR signal is detected, amplified and limited rail-to-rail using an integrated comparator. A synthesized frequency detector block then measures the modulated frequency of the received IR signal. An IR remote control transmits the IR signal of a particular frequency for a fixed duration of 1 second. The digital frequency detector uses a divided version of the system clock and continuously counts the number of clock edges in a pre-programmed 333 ms time window to estimate the received signal frequency. If the determined frequencies of two successive time windows correspond to the same instruction then the signal is considered a valid instruction.

Once a valid instruction is detected the control block takes a corresponding action to change the state of the biosignal monitoring device as illustrated in Table 3.1. A frequency-based encoding scheme was used to avoid the need for complex clock and data recovery to save power. Thus, this technique is limited to a relatively small number of commands; to mitigate this fact the number of programming commands was greatly reduced by implementing a control scheme where commands instruct the device to cycle between different settings as opposed to having many different commands that instruct the device to change to a particular setting. A frequency of 36 kHz increments the mux to select the next recording channel front end for digitization and transmission. Similarly, frequencies of 38 kHz and 40 kHz are used to cycle through the available gain and bandwidth settings. The sensor initially defaults into a reset state (with default gain and bandwidth settings hardwired through external switches) to suit the type of recording desired (neural, ECG, EMG, etc.). Current gain, filter and active channel settings are transmitted with each packet of sample data from the biosignal monitoring device so the user can confirm the device has been programmed as desired.

This implementation allows the device to be programmed from a few meters away while consuming negligible power in the IR receiver (a few microwatts). A tradeoff from using IR as opposed to various RF or near-field communications techniques is the line-of-sight requirement. IR light must have a fairly unobstructed path to the phototransistor to insure

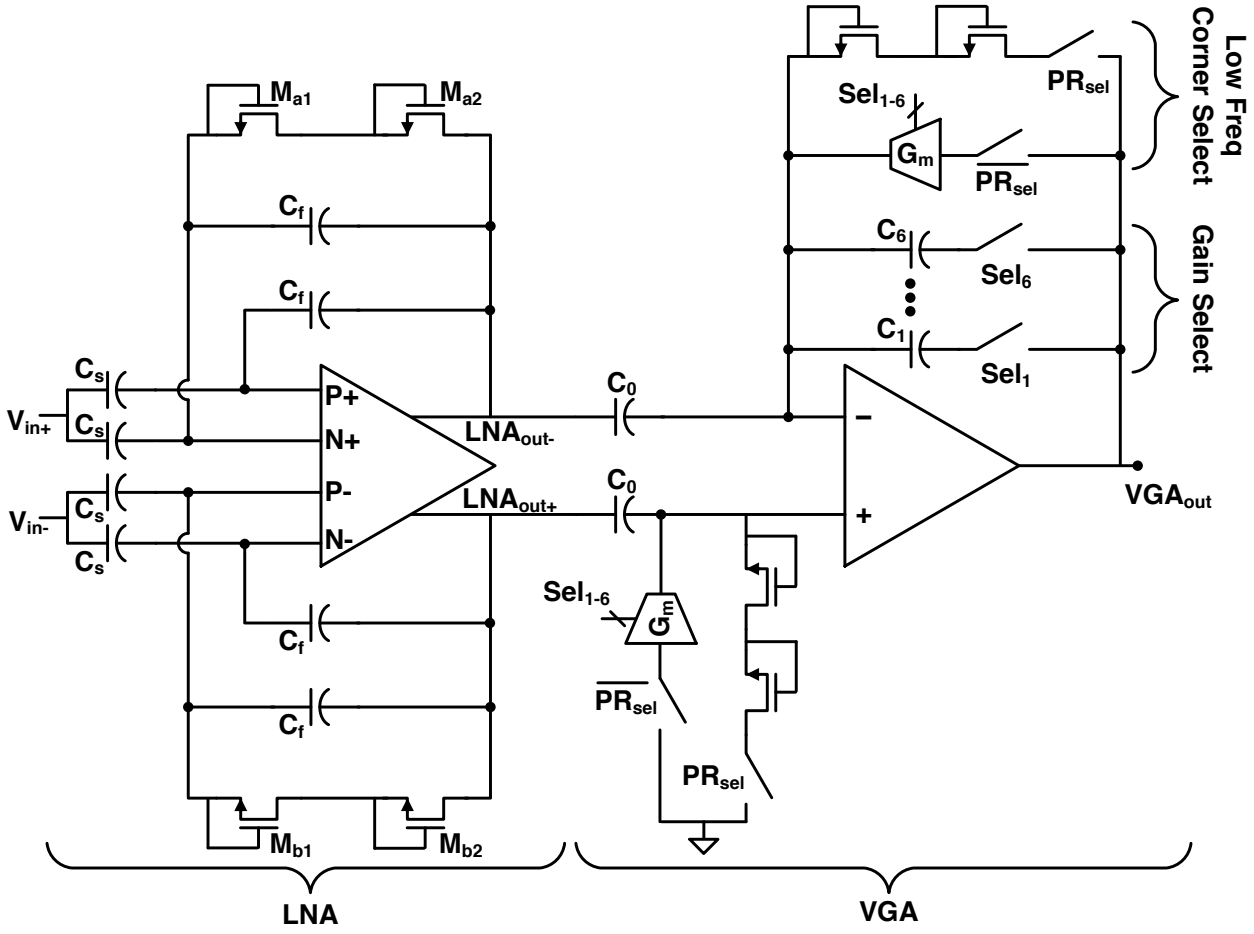

Figure 3.2: Architecture of the fully-differential analog front end.

enough power arrives at the sensor for proper detection. For applications that cannot accommodate this, for example implantations, this receiving method is much less useful since the IR attenuation caused by tissue absorption would greatly reduce the programming distance, possibly enough to make programming impossible all together depending on implantation depth and tissue properties.

3.2.2 Analog Front End

The analog front end (Fig. 3.2) consists of four low-noise amplifiers whose inputs are AC coupled using on-chip 20 pF capacitors. High-resistance (> 100 GΩ) MOS-bipolar pseudo

resistors enable a sub-Hz high pass cut-off frequency [35]. A complementary input stage in which both the n- and pFET's of the input stage contribute to the effective transconductance [36] reduces the input-referred noise voltage by a factor of two for the same bias current [37]. A fully differential closed-loop architecture provides sufficient linearity and supply rejection. Thick oxide MOS transistors are used at the input to minimize the 1/f noise and reduce gate leakage. The VGA consists of a complementary rail-to-rail folded-cascode core with programmable capacitive feedback. Six-level variable gain is set by selecting the feedback capacitors while the seven variable high pass corners are set by programming the feedback transconductor bias current. Each of the four channels is individually configurable for different gain and bandwidth settings. This is useful in single channel deployments to select the best channel and then optimizing the AFE for the recording site characteristics. Table 3.2 illustrates the available gains and their high pass cut-off frequency range covered by the seven filter settings. Four complete analog front ends were included to allow fast switching between channels, not possible by muxing four inputs to a single AFE due to the long settling time of the amplifiers compared to the sampling rate of the device.

Table 3.2: Gain and high pass cut-off frequency options range of the AFE

Gain (dB)	**Filter Corner Range (Hz)**
43	$<0.1 - 230$
47	$<0.1 - 506$
55	$<0.1 - 1100$
64	$<0.1 - 1370$
72	$<0.1 - 1600$
80	$<0.1 - 2000$

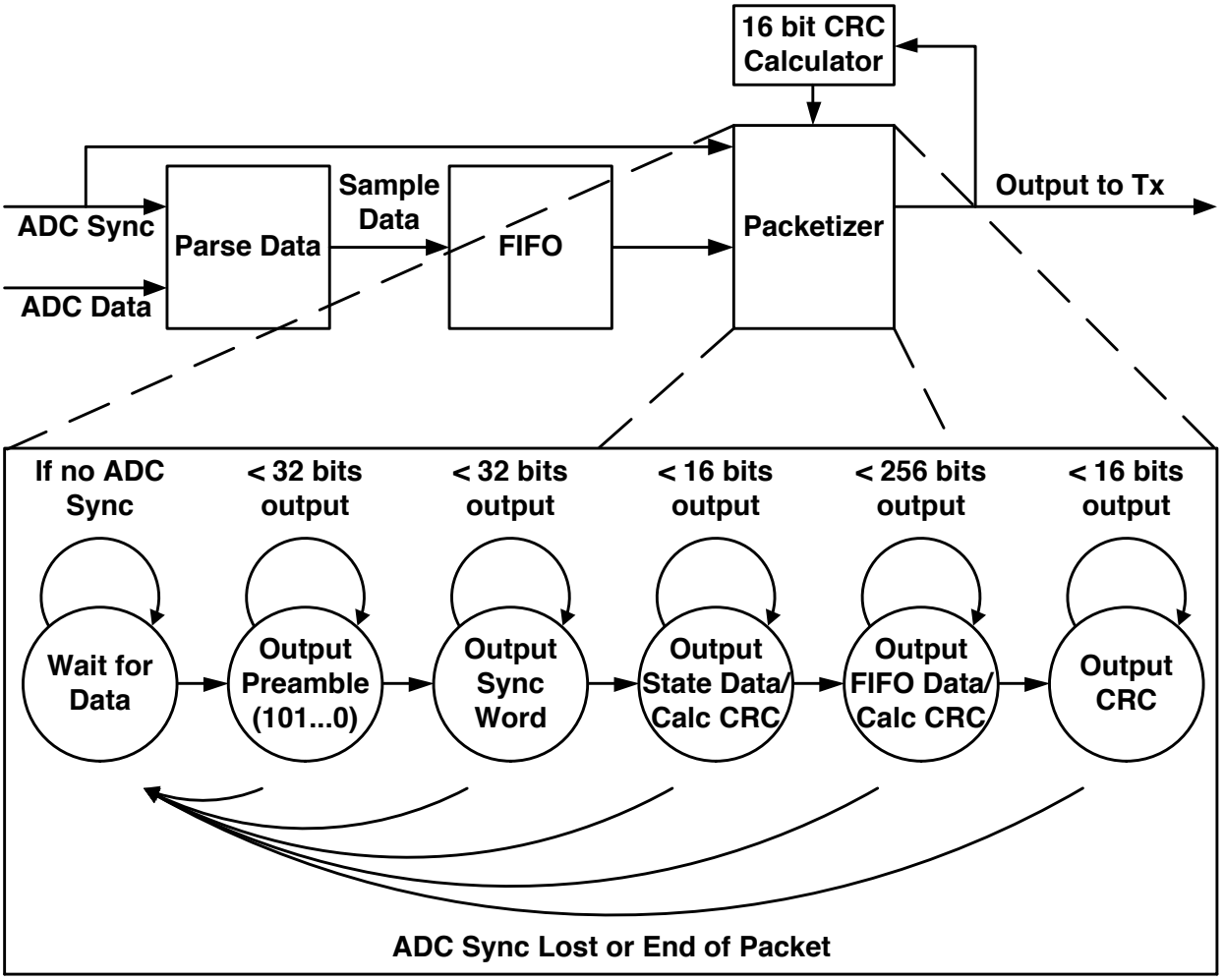

Figure 3.3: Block diagram of packet synthesizer with state diagram of the packetizer block.

3.2.3 ADC and Packetizer

An analog mux selects the amplified signal from one of the four input channels, which is digitized using a low-power 8-bit SAR ADC, designed to operate at sample rates from 10-100 kS/s. The SAR topology was chosen for the ADC to minimize power consumption [36]. Since the AFE settings are wirelessly programmable during operation the user can adjust the gain/bandwidth to provide a close to full swing signal to the ADC, allowing an 8-bit ADC to provide suitable dynamic range for various recording scenarios. The digital ADC output is

read serially from the comparator output. A synchronization signal, which is used internally to purge the DAC capacitor array and SAR logic after each conversion, also synchronizes the serial output. A divider provides the baseband clock for the system from the 48 MHz clock generated in the local oscillator of the transmitter. The divide ratio is programmable to enable different sampling rates depending on the application.

A packet generator block (Fig. 3.3) samples the output of this ADC and prepares the data for transmission. The serial output data from the ADC is buffered in a first-in, first-out (FIFO) memory structure. Data is pulled out of the FIFO by the packetizer block, which inserts this data into a standard packet structure and delivers this packet to the transmitter. The packet header consists of 32 bits of alternating 1-0s, then 32 bits of a constant sync code to identify the beginning of a packet, followed by 16 bits of system state data (current active channel number, gain and bandwidth setting), 256 bits of sample data and finally a 16 bit CRC. This packet structure was designed to be compatible with standard commercial ISM band receivers. The state data and sample data is run through a 16 bit CRC generator concurrently as the packetizer is outputting these bits. This synthesized digital logic block uses 2848 gates and takes approximately 0.018 mm^2 of area.

3.2.4 MICS/ISM-compliant Transmitter

The RF transmitter is typically the most power hungry block in wireless bio-interface systems [38]. We address this by employing a low-power synthesizer architecture that operates entirely at the crystal reference of 48 MHz and drives a 9x frequency multiplying power amplifier (Fig. 3.4), eliminating the need for a PLL/DLL at the carrier frequency [36]. The baseband FSK data directly modulates the reference oscillator using capacitor pulling, allowing a 22 kHz frequency deviation. The reference clock drives a 9-stage DLL, thus the frequency deviation at the carrier frequency of 432 MHz is 198 kHz. This technique can be generalized to other multiplication factors, determined by the number of stages in the DLL and switching legs in the edge-combiner. Both DLL loops must demonstrate sufficient bandwidth to track the FSK baseband signal.

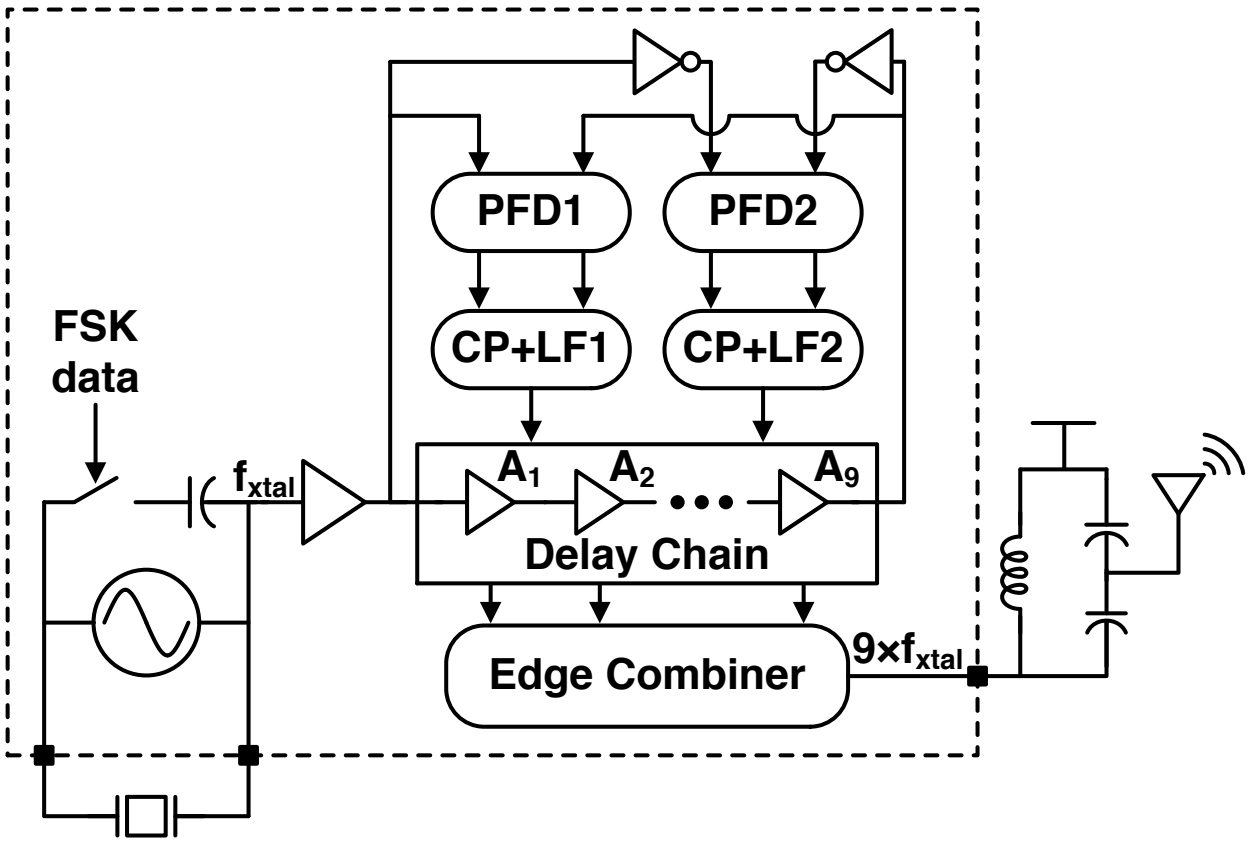

Figure 3.4: Architecture of the frequency multiplying transmitter.

Matching between the delay stages is ensured by balancing the delay-stage loads, symmetric layout and dual-edge locking to minimize reference spurs. The edge-combiner behaves like a high-efficiency, non-linear power amplifier, and produces pulses of current based on overlap of separate delay cells in the DLL. This current is absorbed by a tapped-capacitor LC matching network, which transforms the TX source impedance to match a 50 Ω antenna and attenuates out-of-band spurs. A return loss of less than -10 dB is achieved over the required bandwidth.

3.3 System Characterization and Measurement Results

This IC was implemented in a 0.13 μm CMOS process, measuring (2 x 2) mm^2. Initial testing was performed on a large printed circuit board (PCB) to verify functionality. The die bonded to this test PCB can be seen in Fig. 3.5. The system is intended to accommodate two different battery chemistries: one with a nominal voltage around 1.2 V and another around 1.45 V. With this in mind, the chip was tested with both supplies. Running on a 1.2 V supply, 1.07 mW of power is dissipated by the chip, of which -15.1 dBm (30.9 μW) is transmitted as RF power. With a 1.45 V supply, 1.73 mW of power is dissipated (RF output power of -11 dBm). Phase noise of the transmitter can be seen in Fig. 3.6.

3.3.1 CMOS SoC

Rebooting into a relevant default state is key to this system's ease of use. The IC restarts into a default running state; seven binary inputs are used to set the chip's default AFE gain, bandwidth, and ADC sample rate. These settings are selected through a switch matrix of small SMT pull-up/down resistors on board allowing the same IC to default into appropriate AFE and sample rate states for different recording uses simply by changing these binary inputs. Of course, the chip parameters can be subsequently adjusted using the IR interface described in Section 3.2.1. All settings function as expected.

3.3.2 Deployable System

After benchtop verification, a small, lightweight PCB was designed to facilitate *in vivo* deployment of the system. The biosignal monitor was implemented on a four layer, 500 μm thick FR4 PCB measuring (8.6 x 9.7) mm^2, seen in Fig. 3.7. The top side of the PCB integrates the custom IC, seven 0201 pull-up/down resistor footprints to set different gain, bandwidth and clock speed options for the default state, a reset button, a 48 MHz quartz crystal, an RF matching network, a 17.4 cm long, No. 32 AWG insulated wire serving as a 1/4 λ monopole antenna and an eight pin connector to mate external probes to the

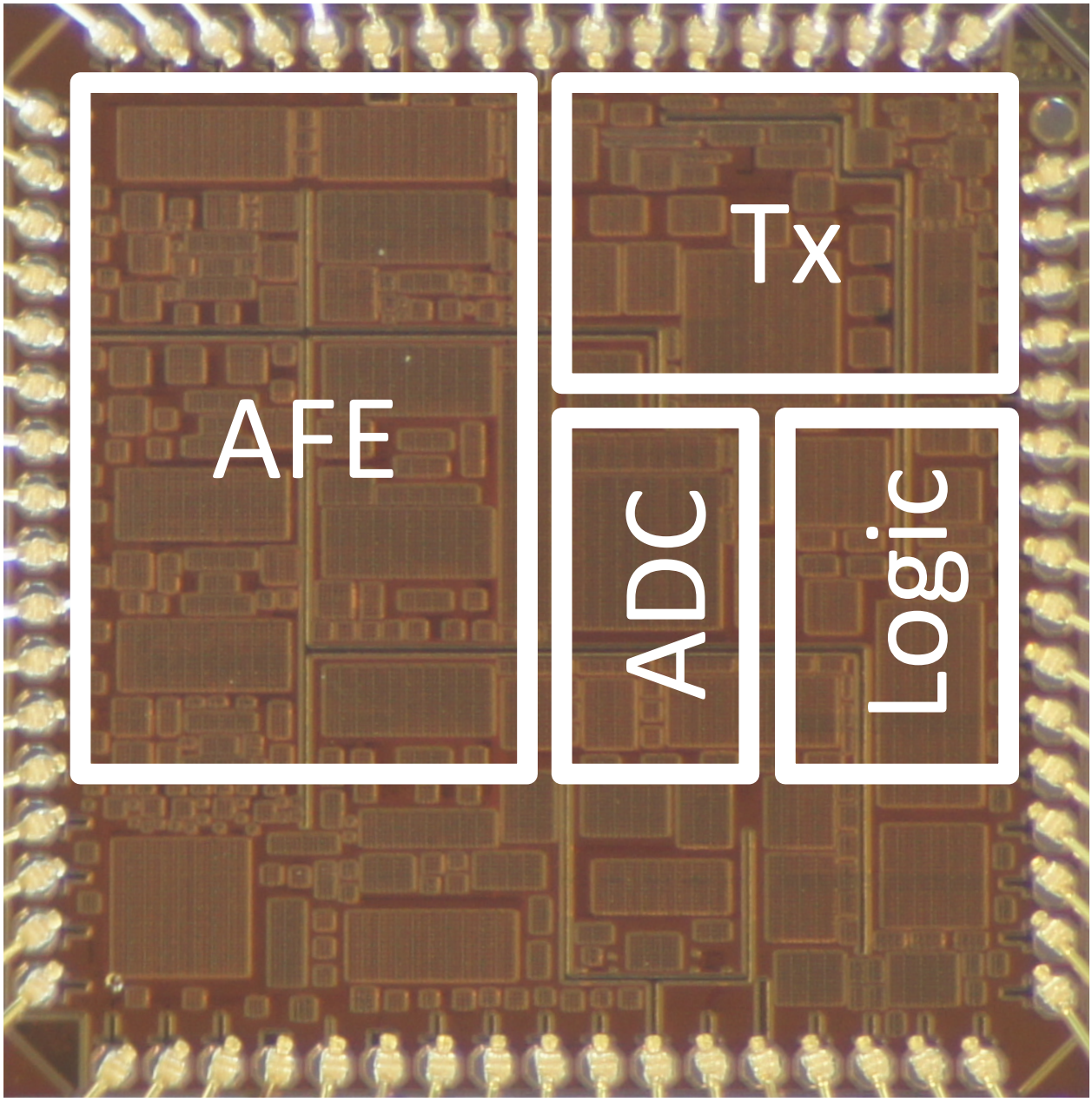

Figure 3.5: Die photo of 2 x 2 mm^2 IC fabricated in 0.13 μm CMOS noting the analog front end (AFE), ADC, transmitter and digital logic blocks.

inputs of the device. Probes connect to this connector via a small flexible PCB that can be custom designed for the given experiment's needs (i.e. single ended or fully differential,

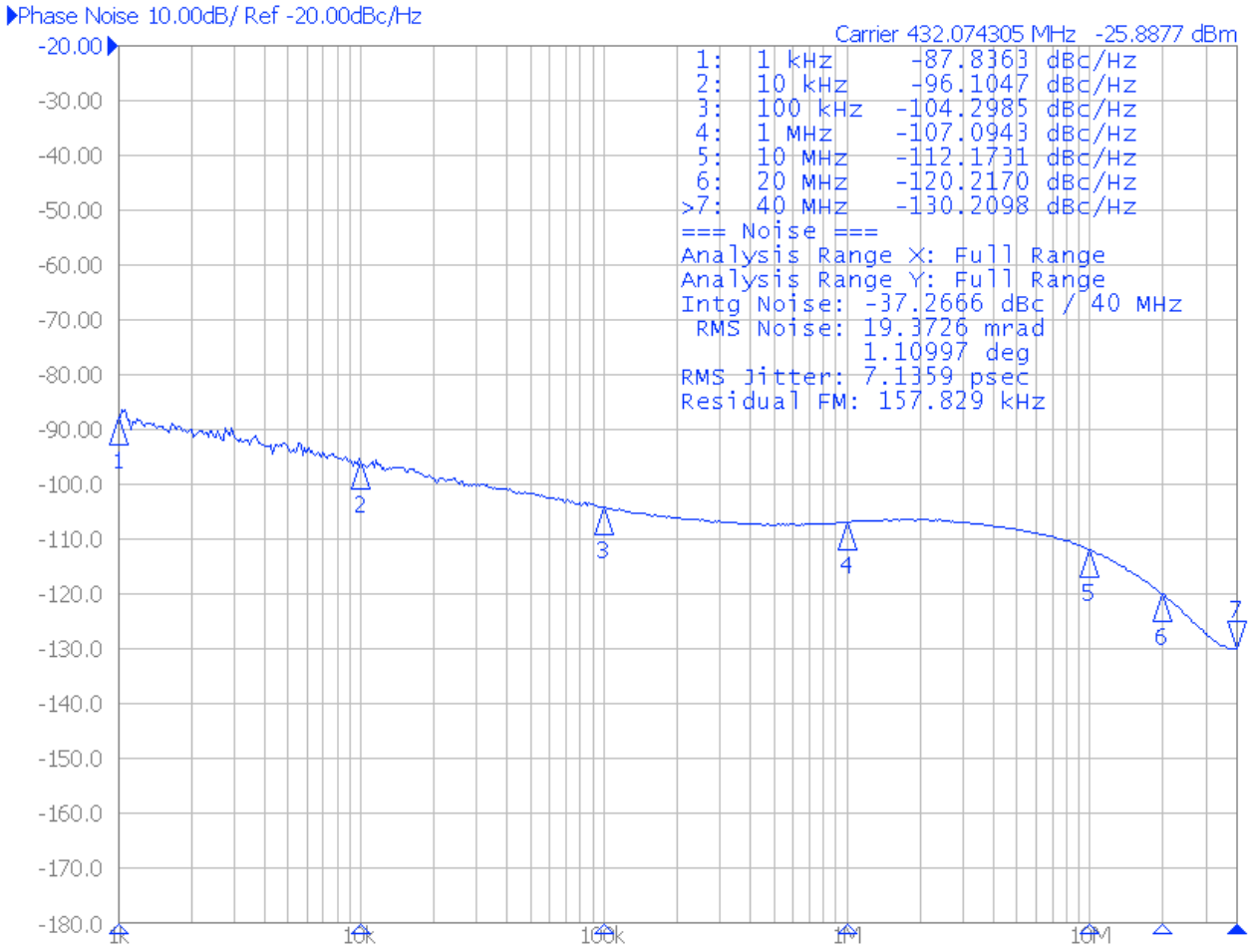

Figure 3.6: Phase noise measurement of transmitter design.

extra attenuation for large amplitude signals, integrated RC filter, etc.), allowing greater flexibility without requiring a re-spin of the biosignal monitor PCB. On the reverse side are either a 4.8 or 5.8 mm diameter battery holder and an infrared phototransistor. The total mass of the device is dependent on which battery is used; loaded with the silver-oxide 337 battery the total system weighs 522 mg including battery and antenna, with the zinc-air size 5 battery and a slightly larger battery holder the system weighs 612 mg.

The seven pull-up/down resistors could be removed to save area at the expense of fixing the default state of the device to only one option. Future versions could integrate non-volatile

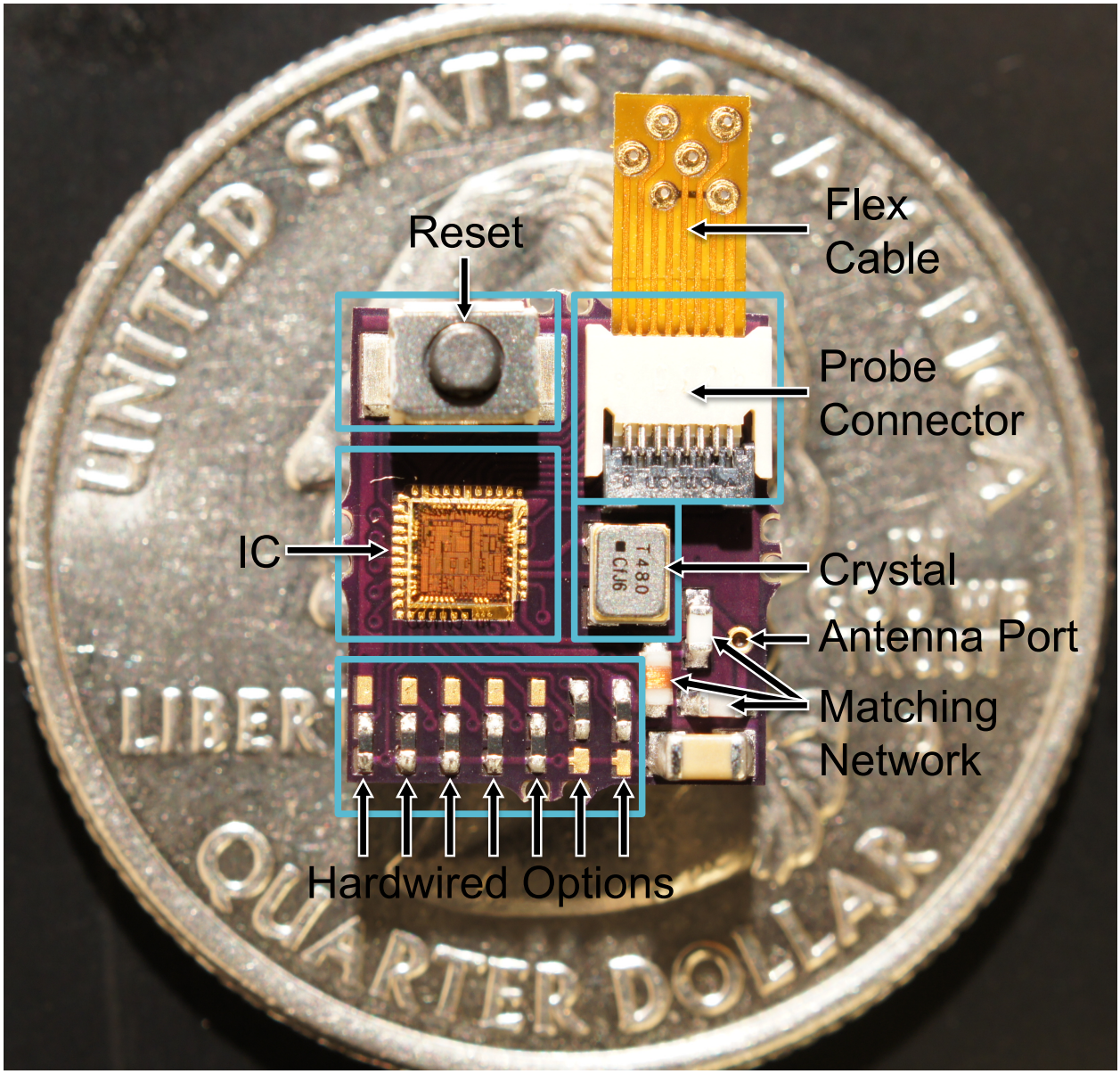

Figure 3.7: Deployable 0.8 cm^2 system and flexible PCB configured for four single ended analog inputs.

memory (NVM) to allow for different default states in the single design by programming the desired state into memory without requiring a reprogramming after every power-on. Likewise, future versions of this device could integrate a power-on reset block within the

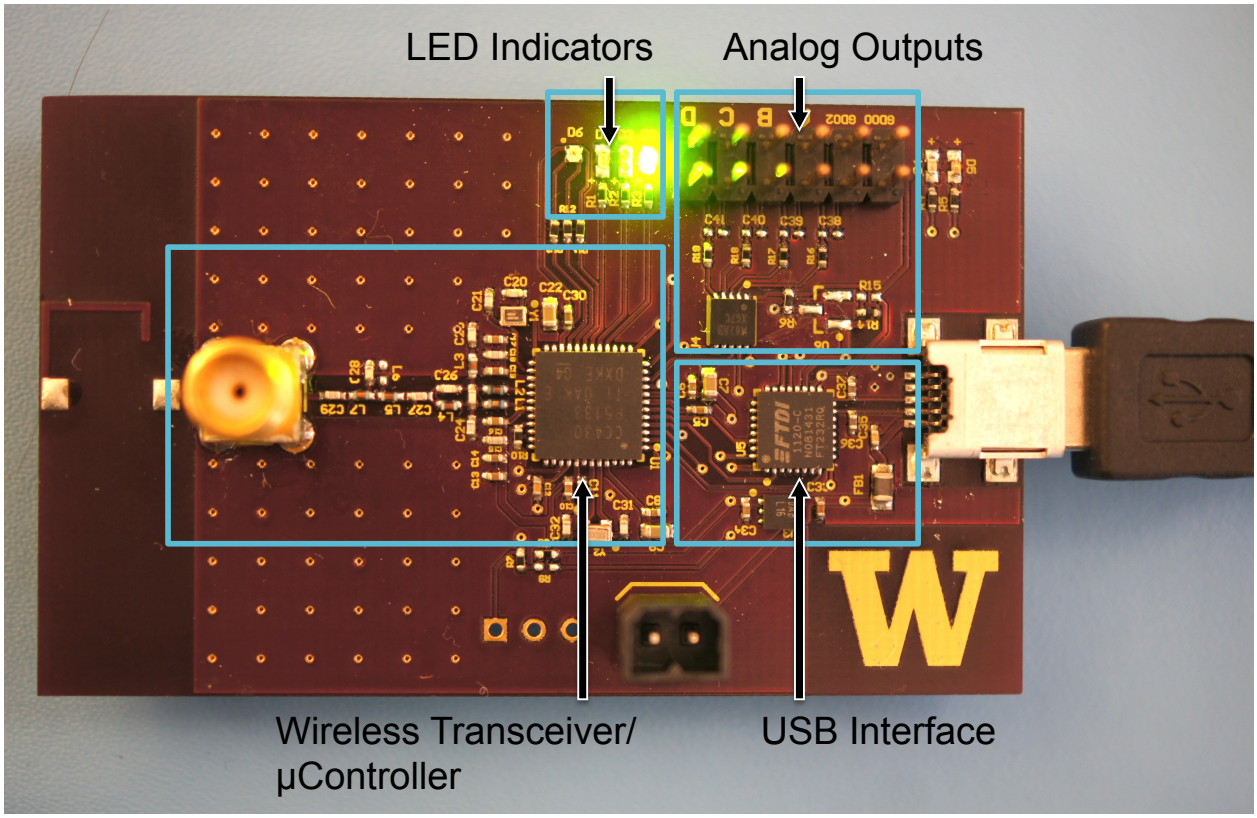

Figure 3.8: Wireless Receiver.

IC, eliminating the need for the external reset switch and reducing total deployable size and weight. The board area of the device is truly limited by the size of the battery and its holder; measuring (6 x 9) mm^2 for the zinc-air size 5 battery holder. Reducing the size any further would require the use of a different battery or an innovative mounting technique requiring a smaller footprint.

3.3.3 Receiver

A companion receiver for the sensor node was designed entirely of off-the-shelf components integrated on a (65 x 40) mm^2 PCB, as seen in Fig. 3.8. On board is a Texas Instruments CC430F5133 microcontroller with embedded wireless functionality, a USB interface translator to stream data to a PC, LEDs to indicate valid data reception, CRC failures and settings

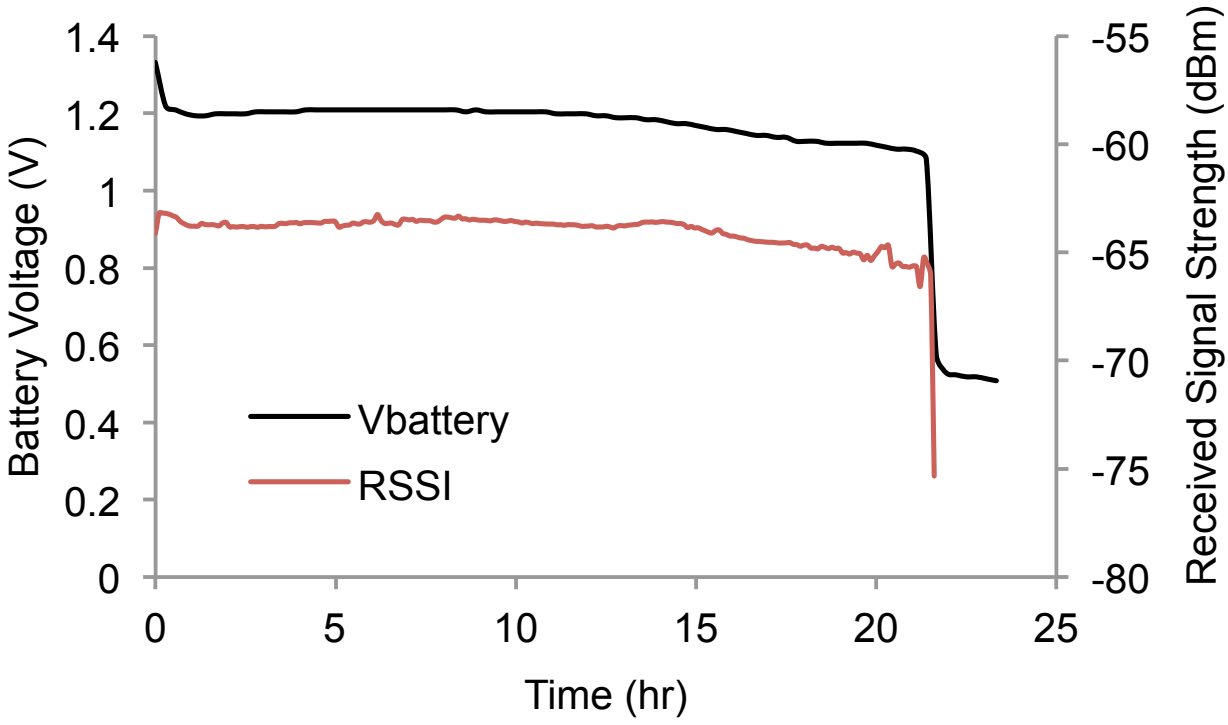

Figure 3.9: Power discharge curve for the zinc-air size 5 battery.

changes due to IR programming and a digital-to-analog converter (DAC) to view the reconstructed analog system in real time via an oscilloscope or audio output. Here we leverage the fact that the sensor node transmits a packet format compatible with this wireless chip, meaning all the build in data processing this chip is capable of can be used in our application, eliminating the need for custom components and greatly reducing the microcontroller code complexity. The receiver board is powered through a PC's USB port so the current consumption of the receiver is not a critical constraint (around 30 mA in this case).

3.3.4 System Characterization

For system deployment, battery choice represents a critical tradeoff between size/weight and energy storage. The IC is capable of operating from a battery voltage anywhere between 0.9 V to 1.55 V. A variety of small coin cell type batteries are commercially available that could

Table 3.3: Small Coin Cell Battery Comparison

Battery Size	**Chemistry**	**Voltage (V)**	**Diameter (mm)**	**Weight (grams)**	**Capacity (mAh)**
337	Silver Oxide	1.55	4.8	0.13	8.3
10	Zinc Air	1.4	5.8	0.32	91
5	Zinc Air	1.4	5.8	0.17	33
CR1025	Lithium	3	10	0.7	30
191	Manganese Dioxide	1.5	11.6	0.8	49
164	Mercuric Oxide	1.4	6.8	0.36	24

power this device, a selection of which can be seen in Table 3.3. Of these, two batteries were chosen that best meet our needs of high energy storage density and a small form factor/low weight, the Zinc-Air Size 5 and the Silver-Oxide Size 337. In both cases the wireless sensor draws more current than these batteries were intended to supply, which limits the amount of energy the system can actually extract from either battery and slightly reduces the nominal voltages from their rated values. Fig. 3.9 shows the battery discharge curve for the Zinc-Air Size 5 battery as well as the received signal strength (RSSI) measured at our receiver board. This battery will power the device for over 22 hours with a fairly consistent voltage of approximately 1.2 V. Over the entire 22 hours of transmission there were 0 packet errors until the final few minutes of operation when the battery was almost completely exhausted.

The total power consumed by the sensor device is 1.07 mW using a 1.2 V supply (nominal Voltage for Zinc-Air 5 battery) and 1.73 mW using a 1.45 V battery (nominal voltage

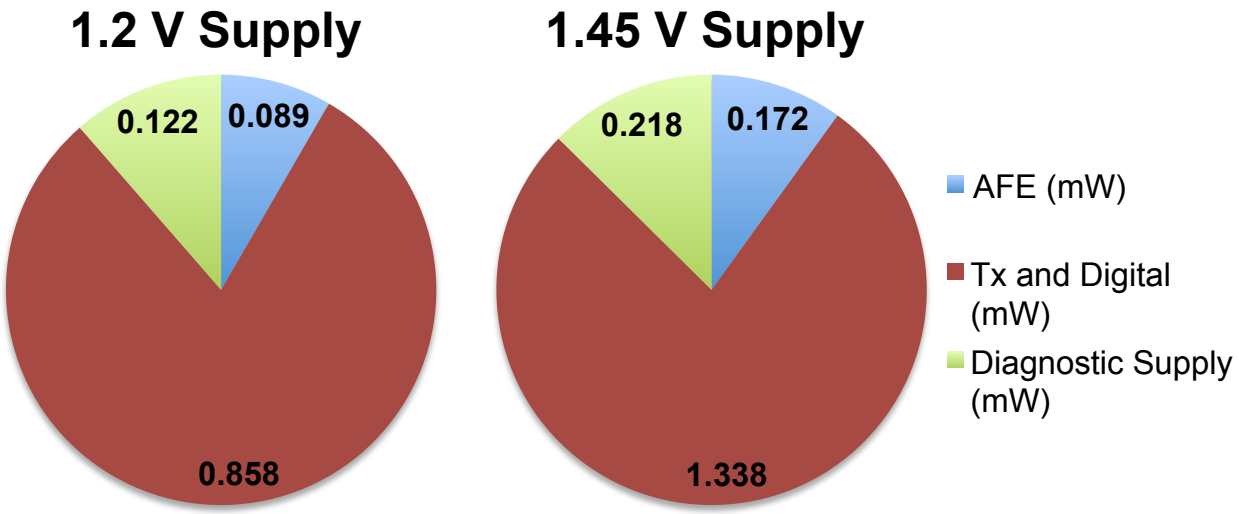

Figure 3.10: Power consumption breakdown using 1.2 V and 1.45 V supplies.

for Silver-Oxide 337 battery). A key digital buffer on the IC was mistakenly powered from a diagnostic supply intended only for debug purposes. It was thus necessary to power this auxiliary supply continuously. This easily fixable design error contributes approximately 12% to the total power consumed by the device. Fig. 3.10 shows a breakdown of power consumption from the different blocks of the IC, including the auxiliary supply pin.

While it is possible to reduce the sampling rate of this device, the transmitter is in a fixed on-state, meaning a reduction in sampling rate will also reduce the baud rate of the transmitter to ensure a 100% duty cycle. Future versions could reduce the sampling rate while keeping the transmitter data rate at a maximum (200 kbps in this implementation), duty-cycling the transmitter as needed, which would greatly reduce power consumption for low sample rate applications. In this version, however, power consumption is fairly independent of sampling rate. Reducing the sampling rate in the current device mainly serves to reduce the total amount of data the receiver/PC would need to process.

Another important metric of any wireless system is the maximum acceptable range for data recovery. Commonly, this distance is defined as the point where the Bit Error Rate (BER, P_b) is 10^{-3}. Packet Error Rate (PER, P_p) can be defined in terms of BER since the

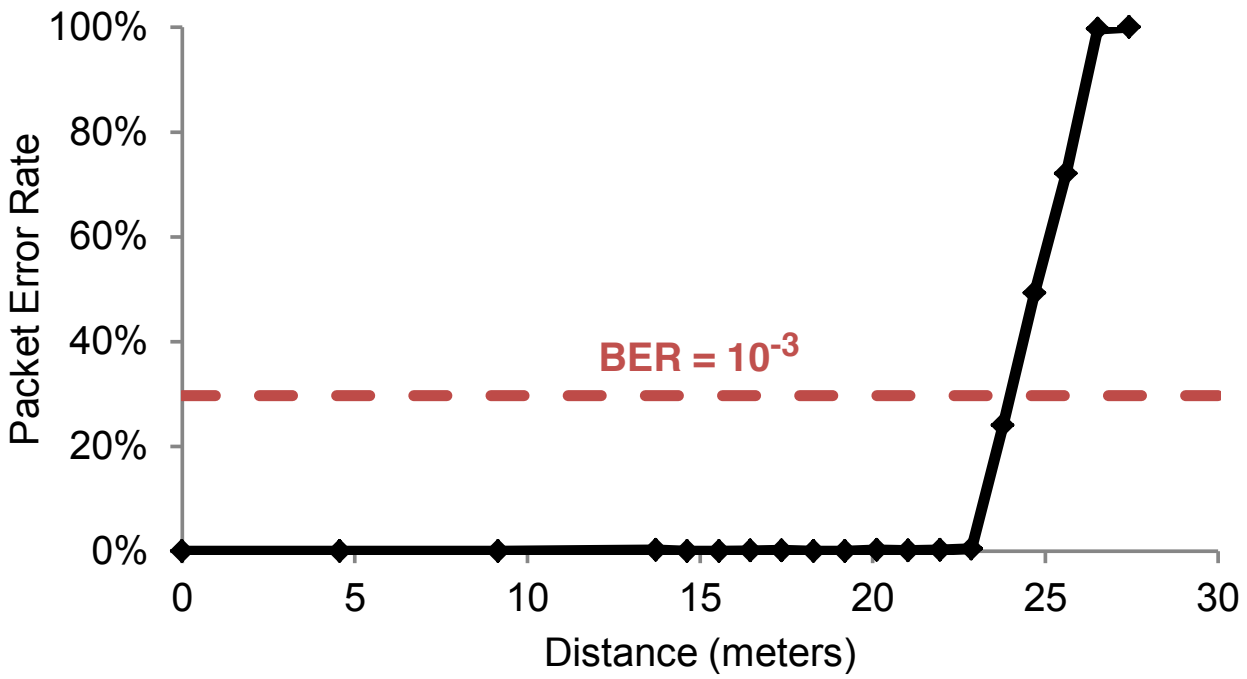

Figure 3.11: Packet Error Rate of the system vs distance between transmitter and receiver.

PER is simply the sum of probabilities of every possible packet error permutation for a given BER. This is shown in (3.1) & (3.2), where n is the number of bits in a packet.

$$P_p(P_b) = \sum_{k=1}^{n} \left[\binom{n}{k} P_b^k (1 - P_b)^{n-k} \right] \tag{3.1}$$

$$P_p(P_b) = 1 - (1 - P_b)^n \tag{3.2}$$

Our packets are 352 bits long; using Equation 1 we see a PER of 29.7% represents a BER of 10^{-3}. Fig. 3.11 shows the recorded PER of the system powered by the 337 Silver-Oxide battery at different distances from the receiver compared to the 29.7% PER point, giving a range of 24 m for this experiment. In a practical situation the acceptable amount of packet/data loss can be quite application dependent. Error detection is done solely by checking the CRC code so one cannot determine which bit(s) is/are in error in this system and thus must throw out the entire packet which makes the data loss in the received data "blocky." Fig. 3.11 can be used to decide the acceptable operating range of the system for

a given application where practical range is decided by how many gaps in the recorded data is acceptable (likely over 20 m).

The total input referred noise of the chip was measured through the entire system shorting the analog inputs to ground and setting the AFE at the maximum gain (78 dB) and widest bandwidth (9.2 kHz) setting (Table 3.2). The received data was then analyzed in Matlab to calculate input-referred noise. The wireless receiver recovered a signal with an RMS value of 1.73 μV and no packet errors. This RMS noise value was computed at the receiver and includes all noise sources, including amplifier noise, VGA noise, ADC quantization noise, aliasing, supply noise, substrate coupling, etc.

3.4 In vivo Testing

3.4.1 Human ECG Recording

A key attribute of this system is its long lifetime (22 hours at 100% duty cycle) and ease of use. Operation requires only inserting a battery and pressing the reset button. This allows it to be easily deployed in a home setting that lacks any support equipment or technical staff commonly available in a laboratory setting that a less refined device might require.

To demonstrate this functionality, the sensor was attached to a freely moving human subject at home over the course of a day, recording the electrical activity of the heart (ECG). Two Ag/AgCl conductive adhesive electrodes were connected in a single-ended configuration to the wireless sensor and attached to the subject's chest who was then left to go about his day while staying within range of the receiver. Fig. 3.12 presents a short length of this ECG data presented on a standard clinical ECG grid showing the expected healthy sinus rhythm. The signal was post-processed with a high order digital 1 Hz high pass filter to eliminate a wandering baseline, a changing dc level common in ECG monitoring likely due to patient movement.

An hour section of this recorded data was further processed, lining up each detected heartbeat with its central spike, known as the QRS complex. 4110 heartbeats were recorded

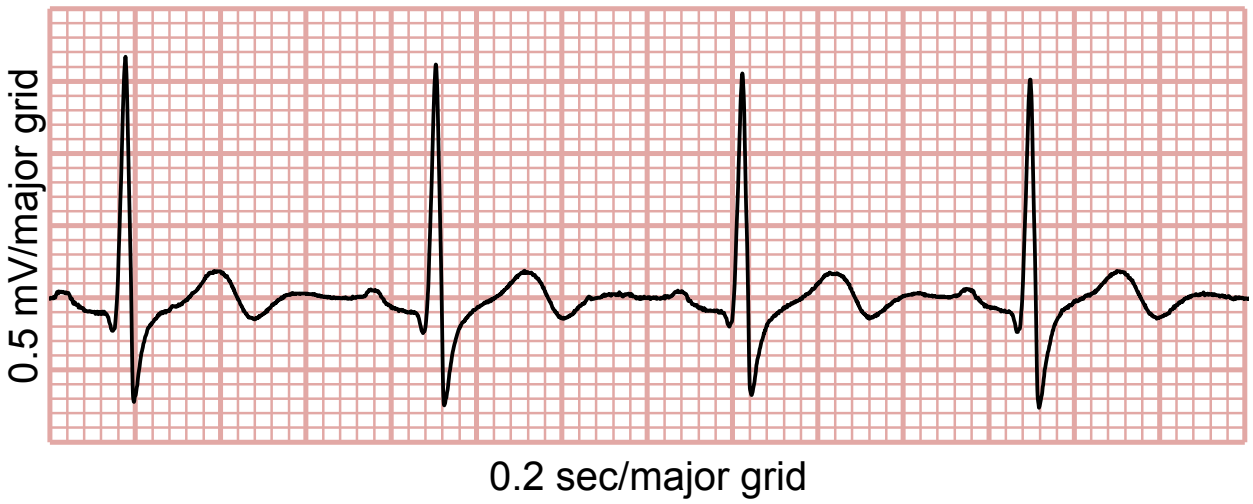

Figure 3.12: Human ECG Recording.

in this hour, which can be seen overlaid in Fig. 3.13. The figure is in a heat-map format, allowing easy visualization of artifacts and heartbeat waveform morphology. The ECG data recorded from a freely moving subject is quite consistent over the length of the experiment, showing only modest changes in the t-wave, the later part of the ECG waveform, which is due to changing heart rhythm as opposed to corrupted recordings.

Lastly, the recorded ECG data was used to determine the subject's heart rate over two hours of normal activity, as seen in Fig. 3.14. There are minor variations in heart rate from beat to beat and over the two hour recording period. Here, 60 heartbeats were averaged together to calculate a mean heart rate for the subject and displayed in a more readable format.

3.4.2 Mouse Single Unit Recording

To demonstrate wireless neural recording from freely moving small animals, extracellular neural recordings from an awake, ambulatory mouse were performed. All surgical procedures were carried out in accordance with the Allen Institute for Brain Science's Institutional Animal Care and Use Committee regulations using sterile techniques. Briefly, the cerebral

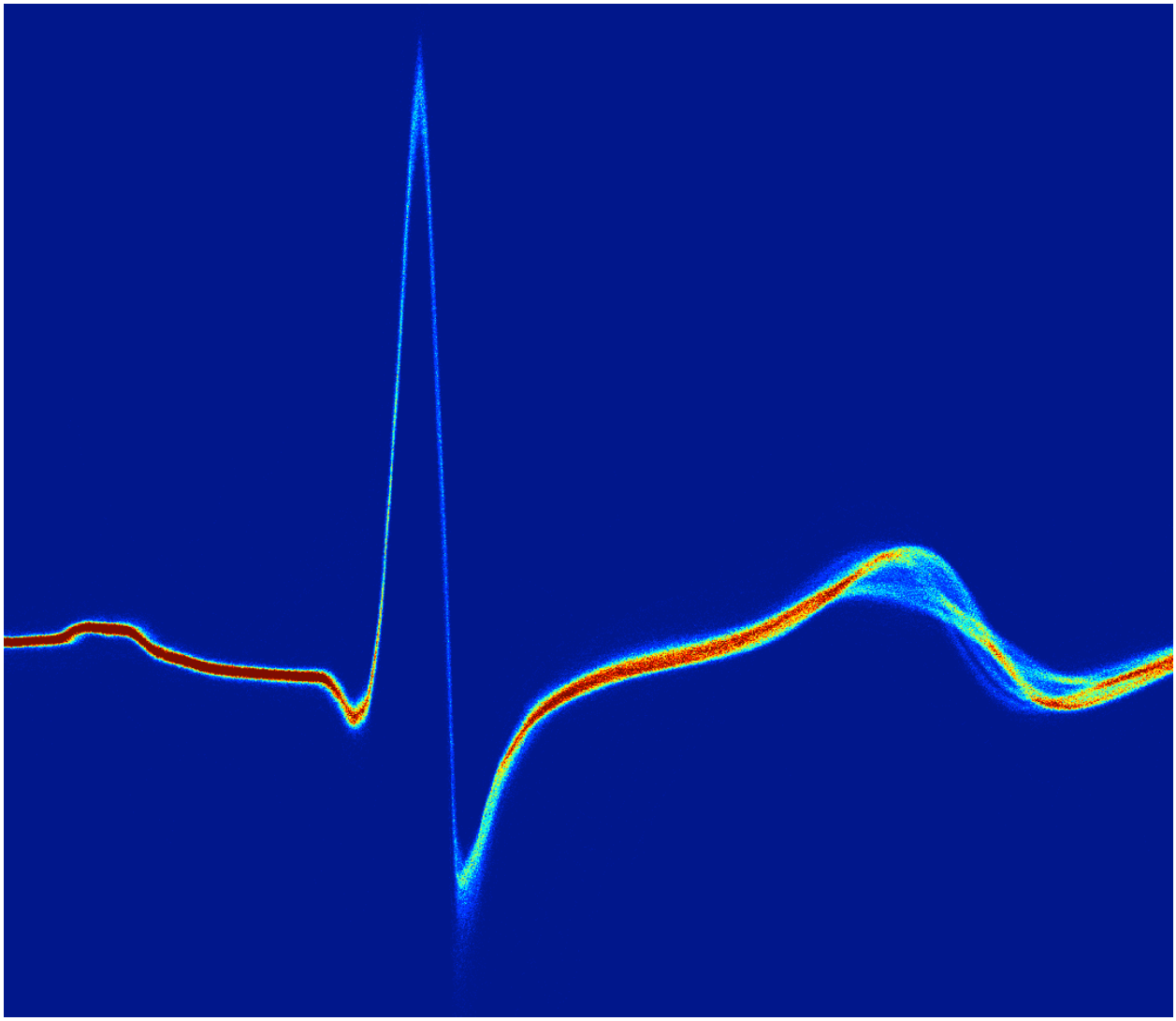

Figure 3.13: Human ECG recording over one hour overlaid.

cortex of anesthetized adult mice (C57/Bl6, 25 g) was implanted with a microwire electrode array, consisting of (4) 50 μm diameter polyimide-coated tungsten wires, [39],[40] coupled to the monitor via a custom flex board (Fig. 3.7). Electrical reference was attached using uninsulated tungsten wire connected to a bone screw in the left hemisphere. Electrodes were implanted into vibrissal somatosensory cortex, which can provide immediate spiking information to researchers via manual whisker deflection [41]. The mouse was allowed to

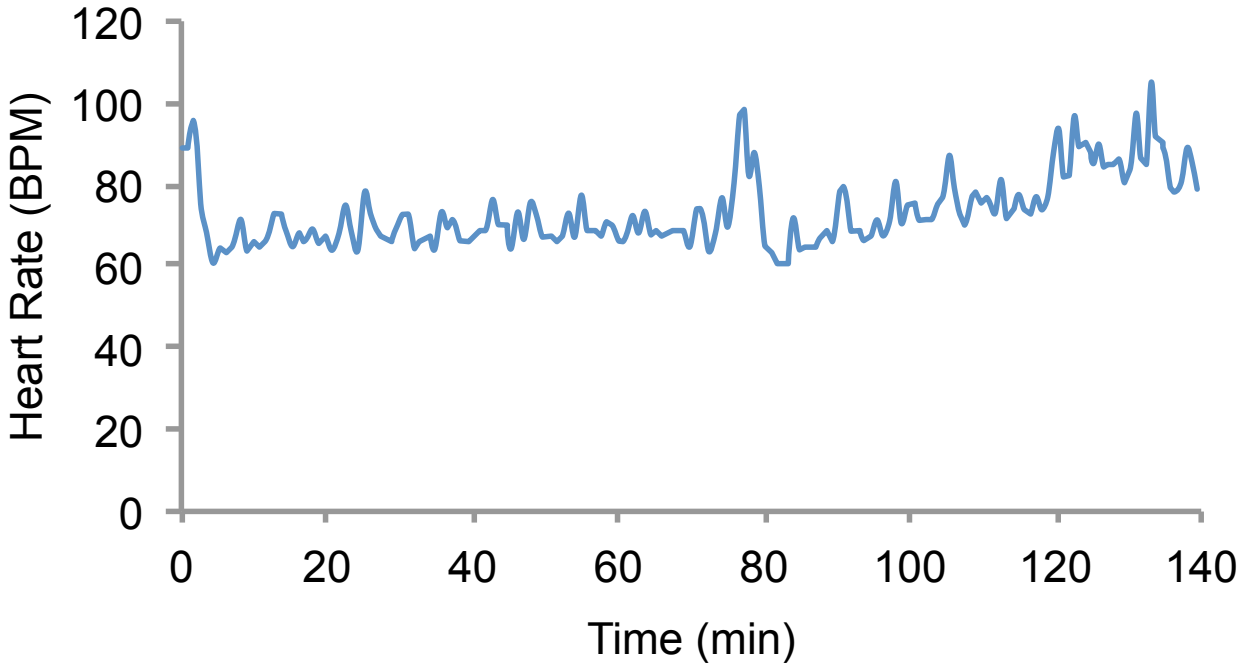

Figure 3.14: Recorded heart rate of human subject over 2 hours of normal activity.

recover from anesthetization before recording response from whisker stimulation, examples of which are shown in Fig. 3.15. Using the IR programmer the one electrode of four implanted closest to the cells of interest was exercised post-surgery by cycling through all four channels and recording from channels with active spiking. Likewise, the IR programmer was used to set the gain of this channel to utilize as much of the dynamic range of the ADC as possible without clipping the signal. This method of fine-tuning the recording session would be much more difficult with a wired or near-field communications system since the test subject is freely moving and is not easily held still to keep wires (or inductive coupler, etc.) attached.

With antenna and battery, the entire neural recording system weighed only 612 mg, and continuously streamed neuronal spiking data from freely moving mice for up to 22 hours. Such a system is capable of replacing large and complicated recording equipment, placing the technique of extracellular electrophysiological recordings into a wider variety of laboratories with limited space or resources. Data transmission was recorded at distances over 10 m

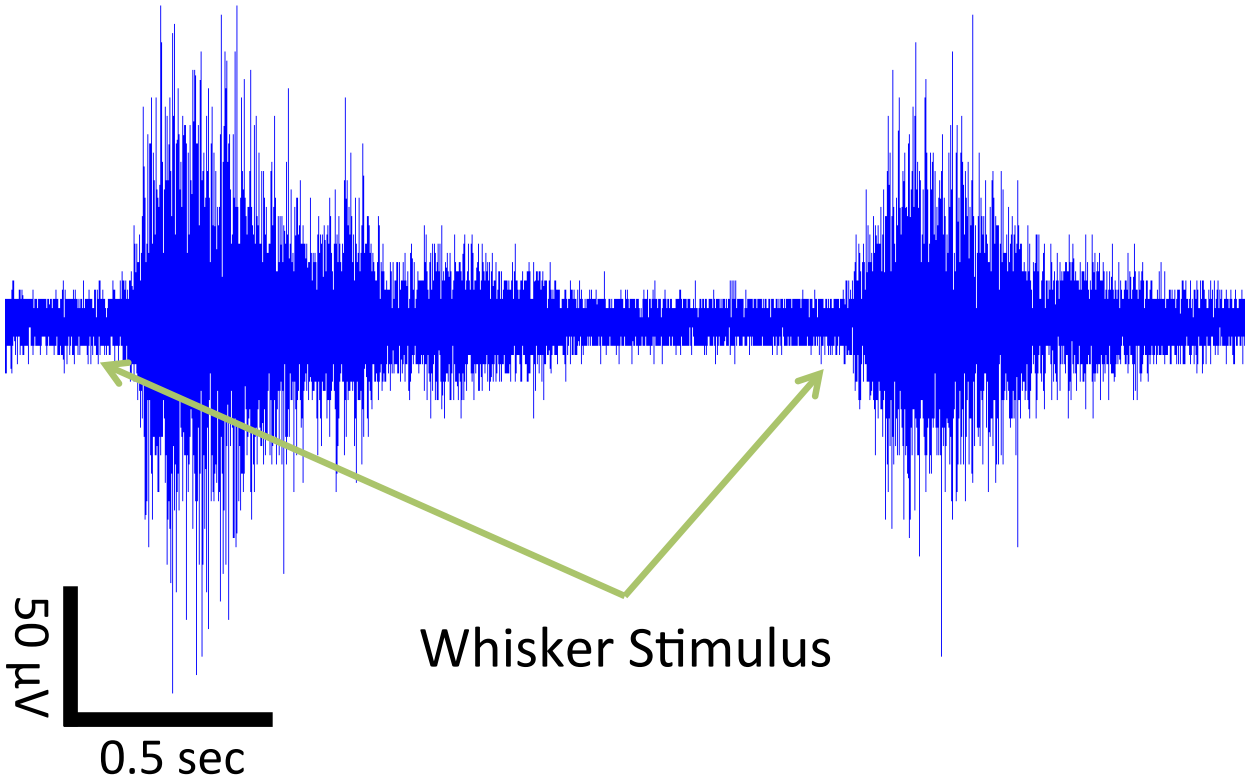

Figure 3.15: Spike recording stimulated in response to whisker deflection.

with a USB-PC receiver interface. Sensory-evoked neural spiking data recorded wirelessly were found to be qualitatively comparable to data recorded in a conventional wire-tethered recording system.

At least two individual firing neurons could be identified from recordings in the somatosensory cortex of a freely moving, awake mouse, when this spike data was processed with sorting software ([42]). These two spike waveforms, shown in Fig. 3.16, are displayed in a similar heat-map plotting technique to Fig. **??**. Since these two neurons were firing at approximately equivalent intervals their waveforms interact and corrupt a single spike waveform. When we overlay all the spikes in this heat-map format however, the spike shape is clearly visible.

3.5 Conclusion

Chapter 3 demonstrates a low-power wireless biomedical sensor suitable for large-scale deployment in mainstream as well as experimental medical applications. The system requires minimal human calibration, in the form of a reset switch to start the recording, and operates continuously for 22 hours from a single zinc-air battery. A receiver comprised of off-the-shelf components records the transmitted digitized data from distances of over 20 m. A simple IR wireless programmer allows amplifier settings to be changed during recording if needed to further fine-tune the setup. The entire biomedical wireless sensor consumes 1.07 mW from a 1.2 V supply.

The system's ease of use allows it to be used in settings outside a laboratory and requires no technical knowledge to operate. To demonstrate this, the system was deployed in a home setting recording ECG and heart rate from a human over multiple hours without any need to tinker with the system. Highly configurable amplifiers make this system suitable for a wide range of recordings/experiments in addition to home monitoring. In addition to ECG recording, this system was used to record single neuron action potential firings within the brain of mice. The low weight and size of this device is beneficial for such small animal experiments, providing the experimenter with a way to record neural activity without weighing down the animal or confining it with a classical tethered system.

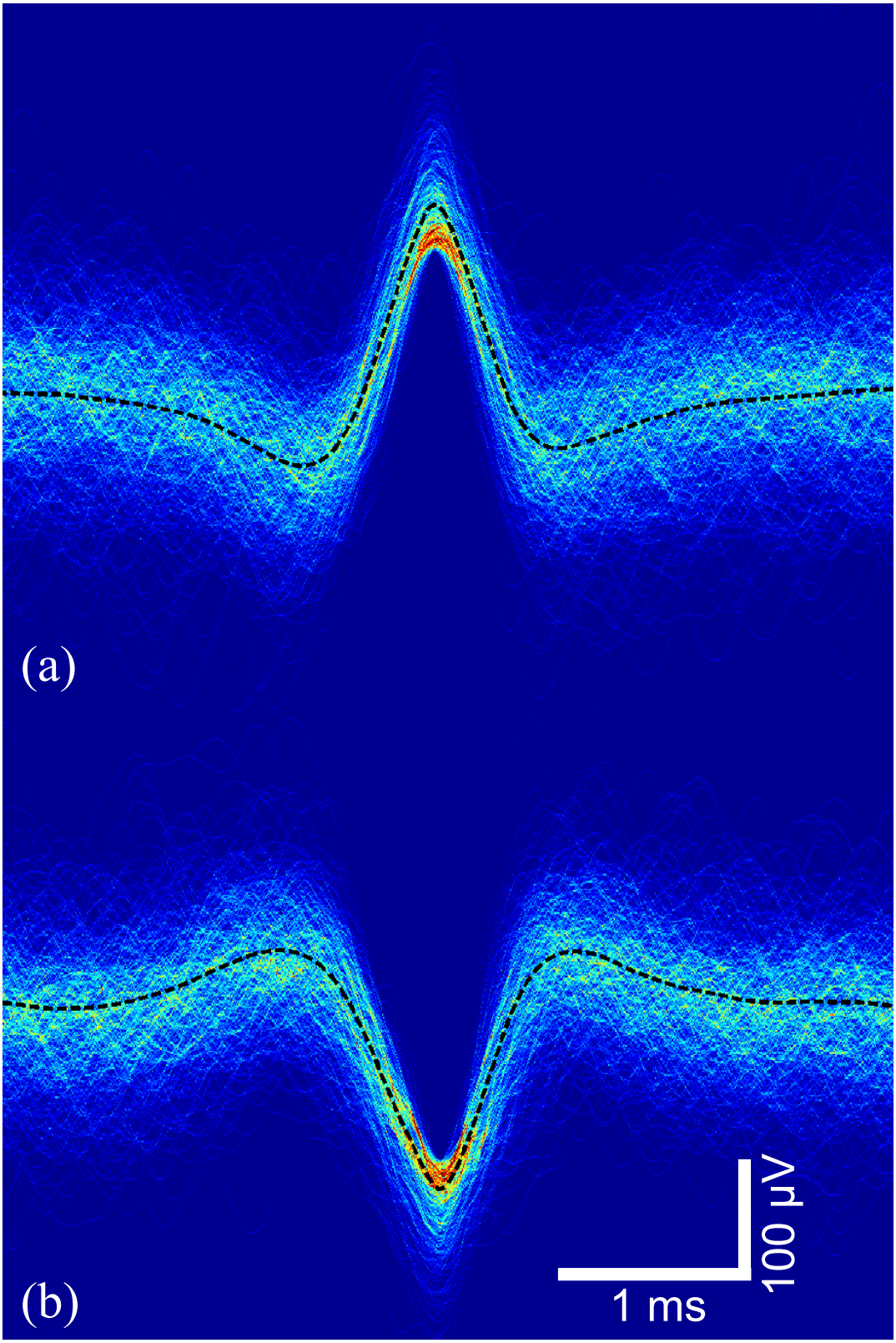

Figure 3.16: Overlaid spike recordings of at least two firing neurons, (a) and (b).

Table 3.4: Comparison to Prior Work

	[26]	[27]	[28]	[29]	[30]	**This work**
Supply voltage	1.8 V	3.0 V	3.0 V	1.5 V	1.65 V	1.2/ 1.45 V
Power consumption	36 μW	3.6 mW	-	1 mW	6 mW	1.1/ 1.7 mW
Approximate size	22 x 17 mm^2	13 x 9 mm^2	16 x 17 mm^2	6 x 5 mm^2	8.8 x 7.2 mm^2	8.6 x 9.7 mm^2
Total mass	1.6 g	0.79 g	4.5 g	0.17 g	-	0.61/ 0.52 g
Battery life	wireless	2 h	6 h	5 h	-	22.3/2 h
Signals transmitted	1 neural	2 neural; 2 EMG	15 neural	2 neural; 2 EMG	128 neural	4 Variable gain/ bandwidth
Sampling rate	8 kS/s	1.92-11.52 kS/s	50 kS/s	1.92-11.52 kS/s	640 kS/s	9.1-18.2 kS/s
RF frequency	915 MHz	920 MHz	3.05 GHz	902 MHz	-	432 MHz
RF modulation	backscatter	digital FSK	FM	digital FSK	UWB	digital FSK
RF datarate	9.6 kbps[1]	345.6 kbps	-	345.6 kbps	90 Mbps	200 kbps
RF range	1 m	$\sim$2 m	4 m	$\sim$2 m	-	$>$20 m
Wireless programmability	none	none	none	none	none	Gain: $43-80$ dB HPF: $0-1.5$ kHz
Requires receiver tuning	no	yes	no	yes	yes	no
Tested animal(s)	moth; primate	locust; elec. fish; dragonfly	mouse	dragonfly	snail	human; mouse; moth
Publication year	2009	2010	2011	2011	2009	2012

[1]Varies with range

Chapter 4

12-CHANNEL MULTIPURPOSE WIRELESS BIOSIGNAL MONITOR

4.1 A Single-chip Encrypted Wireless 12-Lead ECG Smart Shirt for Continuous Health Monitoring [43]

An electrocardiography SoC is integrated into a form-fitting textile along with flexible electrodes, battery and antenna. Clinically standard 12-lead ECG is recorded from this smart shirt. The data is encrypted and wirelessly transmitted via an on-chip ISM band radio and flexible antenna allowing secure, continuous cardiac monitoring on a smartphone while dissipating less than 1 mW.

4.1.1 Introduction

Advances in low power chip design will enable new applications in the wearables space. It is likely that these advancements will have a profound influence on healthcare. Section 4.1 presents a smart shirt that performs all-day wireless transmission of clinically-standard 12-lead ECG signals for cardiac monitoring. It is built upon a single-chip platform consuming sub-mW power for wireless clinical 12-lead ECG and 95μW for wireless heart rate monitoring. We have designed and fabricated a custom shirt containing dry electrodes, our IC, and a flexible antenna to demonstrate high fidelity ECG recording from a healthy human subject. The entire electronics package (chip + antenna + battery) is flexible and less than 2.3 mm thick throughout, allowing easy integration into various textiles. Our goal is to make this technology inexpensive enough for incorporation into consumer-grade clothing with continuous and secure connectivity to smartphones.

Wired systems necessitate tethering patients to equipment or logging data for later down-

load, limiting mobility or delaying potentially life-saving alerts. Advances in textile electrodes have allowed for the development of highly integrated smart shirts [44], leaving the size of the electronics as the major hurdle. To address these problems, weve combined all needed systems for wireless ECG into a single chip (4.1) enabling low profile textile integration.

4.1.2 Design

Dry electrodes couple human heart potentials from their clinically relevant positions (RA, LA, RL, LL, V1-6, Fig. 4.1.2) to the chip via 12 independent, fully differential channels which are digitized, encrypted and transmitted wirelessly using an on-chip low power 433MHz FSK transmitter. The gain of each of the 12 channels is programmable between 40-80dB independently to allow each channel to use the full dynamic range of the 8-bit SAR ADC for various signal levels [25]. A 200kHz system clock and ADC overhead result in a sample rate for each ECG channel of 1.52kS/s. A low-voltage bandgap reference generates a 0.5V reference for two on-chip low-drop linear regulators (LDOs). The LDOs provide separate 1.0V power supplies for the analog and digital portions of the chip.

The transmitter is the dominant source of power consumption in many low power wireless systems. We use an increased datarate version of our frequency-multiplying transmitter [21] to allow this system to transmit all 12 channels in real-time. Total chip power consumption of less than 1 mW enables all-day transmission of data using a rechargeable 20 mAh V20HR, 11.5mm diameter, 2.3 mm height coin cell.

Protecting the privacy and security of health data is critical given the upcoming proliferation of wearable wireless healthcare devices. We have integrated a 128-bit Advanced Encryption Standard (AES) cypher into our chip, which encrypts all wireless transmissions to combat the theft of sensitive data. 48 bytes of encrypted data are combined with system info (AFE settings, mode of operation, etc.) and a CRC check to create a standard packet format compatible with commercially available receivers.

We have designed and fabricated a comfortable garment that integrates our single chip system, a flexible patch antenna, and a full set of 12-lead ECG dry electrodes into a smart

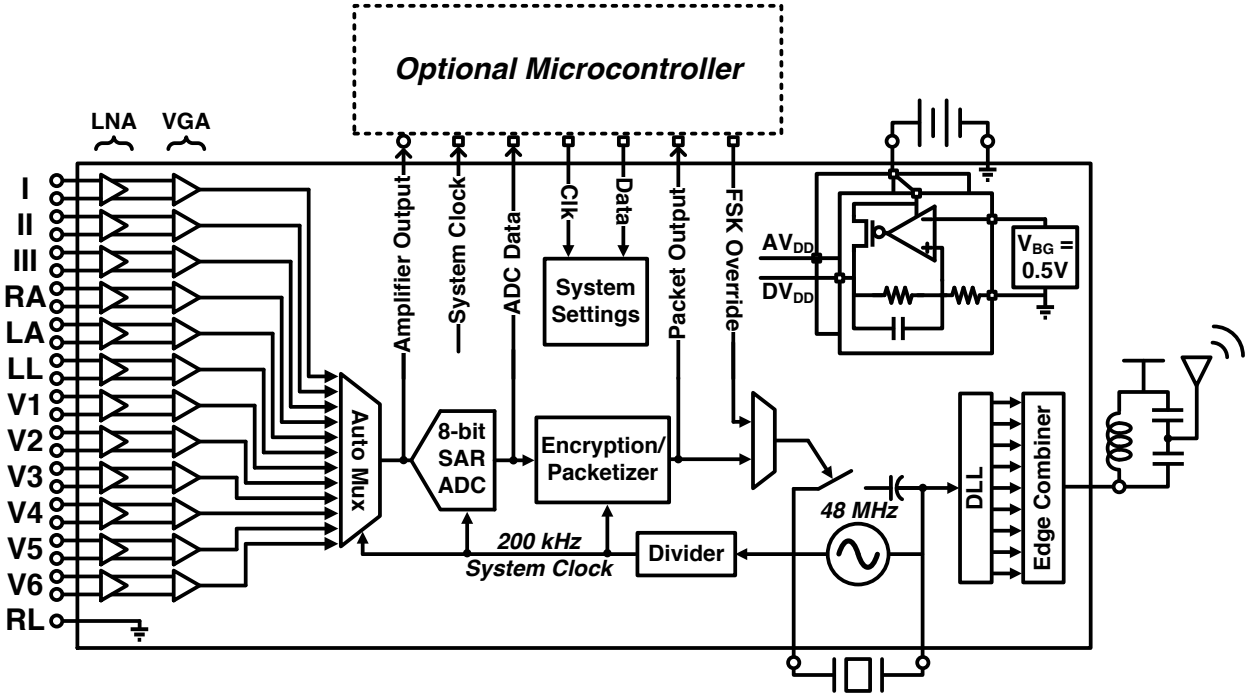

Figure 4.1a: System block diagram of the ECG SoC.

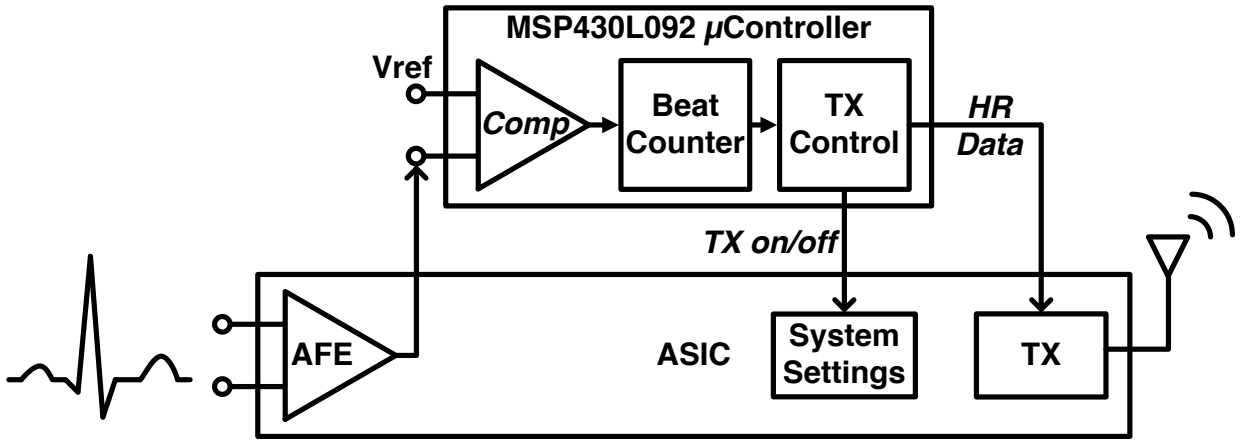

Figure 4.1b: System block diagram of the heart rate monitor implementation.

shirt (Fig. 4.1.2) by modifying an athletic compression shirt [45]. ECG recording requires electrodes placed on documented areas on the human torso to ensure standardized signals for

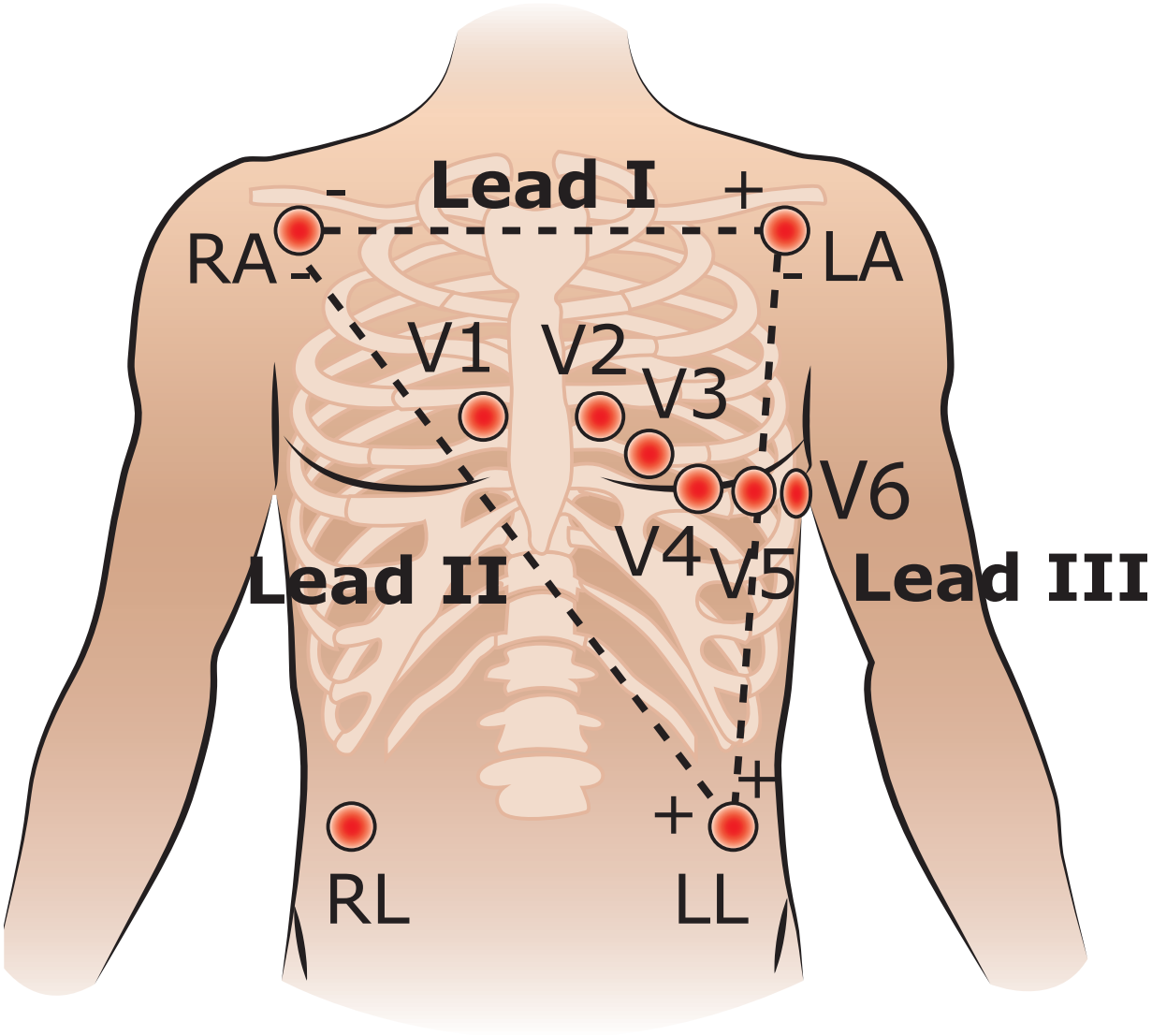

Figure 4.2a: 12-lead ECG electrode placement.

Figure 4.2b: Constructed smart shirt with embedded electrodes and electronics.

clinicians and heartbeat analysis algorithms. Dry, non-adhesive electrodes are employed for shirt reusability and comfort. Commercially available electrodes from a heart rate monitor manufactured by Polar USA were attached inside the shirt. Shielded, thin coaxial wires (810 μm in diameter) are sewn into the shirt to connect the IC to the electrodes. The IC, flexible PCB, battery, and flexible patch antenna are contained in a small pouch on the chest that is 2 mm in max thickness. The 433 MHz patch antenna is 100 μm thick and extremely flexible/conformal.

4.1.3 Results

Data is wirelessly transmitted to a small receiver dongle using only off-the-shelf ICs that interfaces with a laptop or smartphone via USB for display/processing. The shirt records, digitizes, encrypts, and wirelessly transmits accurate 12-lead ECG recordings reliably up to 10 m from the body. The measured RF power at a range of 1.5 m with the system on-body is shown in Fig. 4.3, verifying that the shirt system can easily communicate with nearby devices (e.g. cellphone in a pocket). 4.4 is a 2-second clip of data in a clinically standard ECG grid displaying all 12 waveforms, which were recorded simultaneously from the shirt worn by the author several meters away from a wireless receiver. These signals were filtered using a digital high pass filter with a 1 Hz corner to eliminate any DC shift due to movement of the patient.

By default, the chip boots into full-rate 12-lead ECG streaming mode at power-up. In addition, we designed a flexible interface into our chip (Fig. 4.1) that can be utilized by a microcontroller to modify the signal path and duty cycle, as well as perform signal analysis. For example, we can reprogram the shirt to perform simple heart rate monitoring where only one channel (Lead II) is active. The microcontroller extracts heartbeats and enables the transmitter periodically to broadcast timing data. Limiting the active time of the transmitter (0.08%) changes this same IC from a 12-lead ECG recorder to a low power wireless heart rate monitor consuming 95 μW (Fig. 4.5).

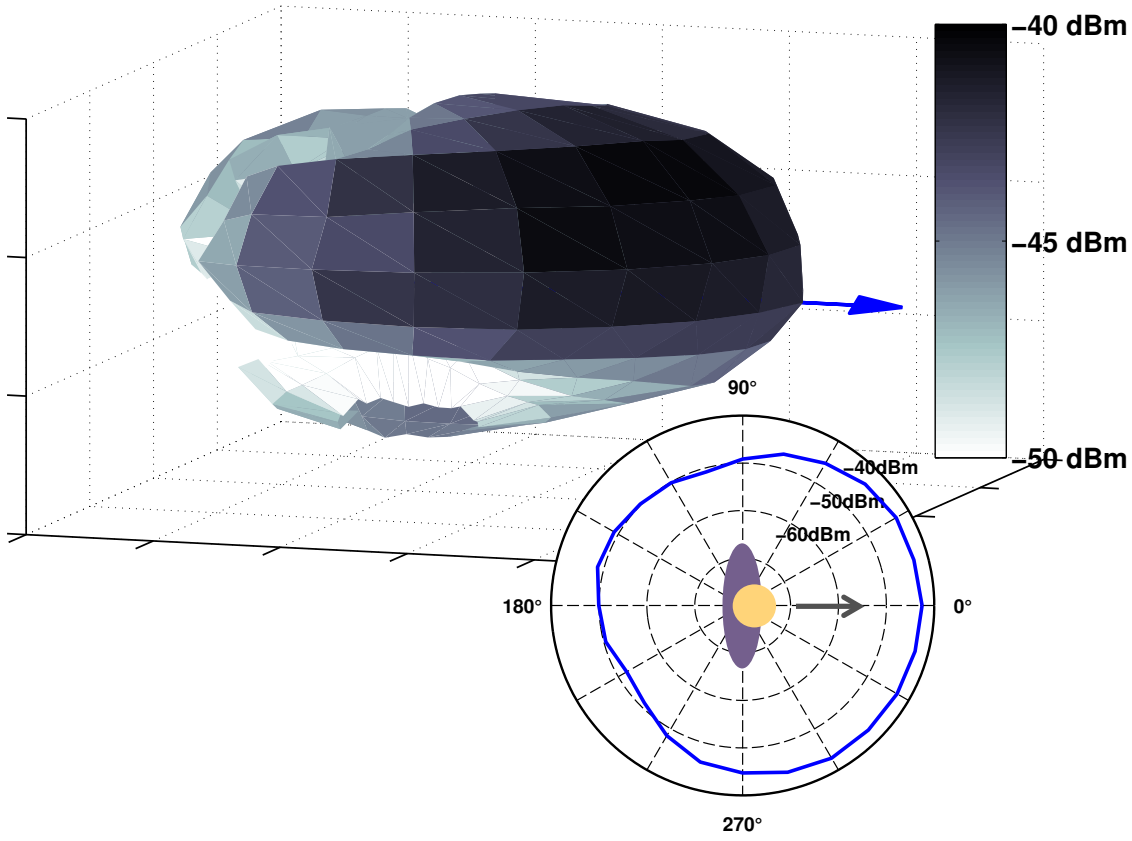

Figure 4.3: Smart shirt 433 MHz radiation pattern in 3D space as well as in the horizontal plane (front of the shirt to the right).

4.1.4 Conclusion

We have demonstrated a wearable, sub-mW 12-lead ECG system. A prototype shirt was constructed as a proof of concept demonstrating the potential of this low power SoC. It can accomplish continual transmission of the entire 12-lead ECG signal ensemble all day powered by a small coin cell battery within the shirt. Since the system is integrated onto a single chip the unit cost of the device can be made extremely low, providing a path towards ubiquity of wearable health monitors in common clothing.

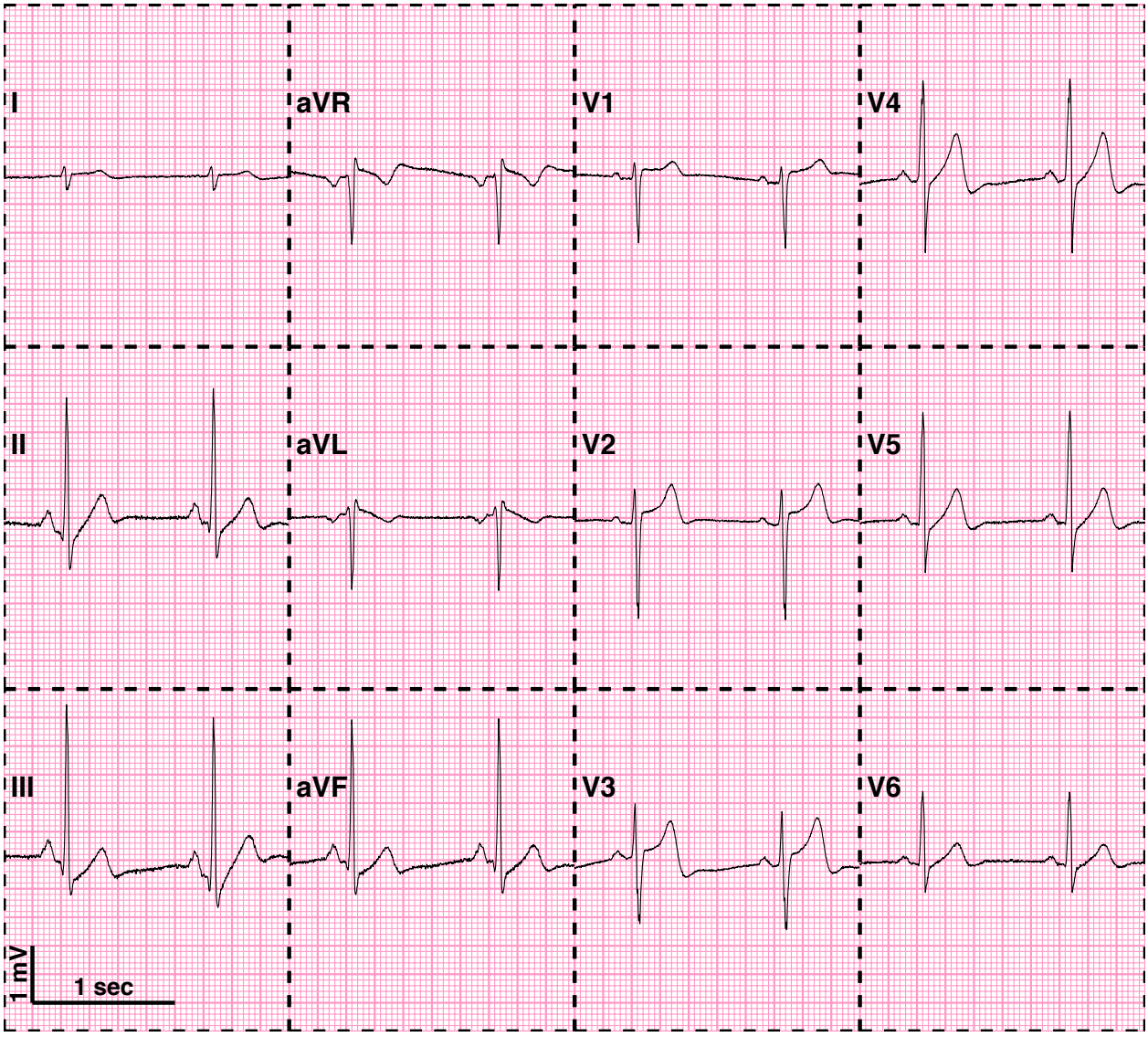

Figure 4.4: Two-second section of 12-Lead ECG recording.

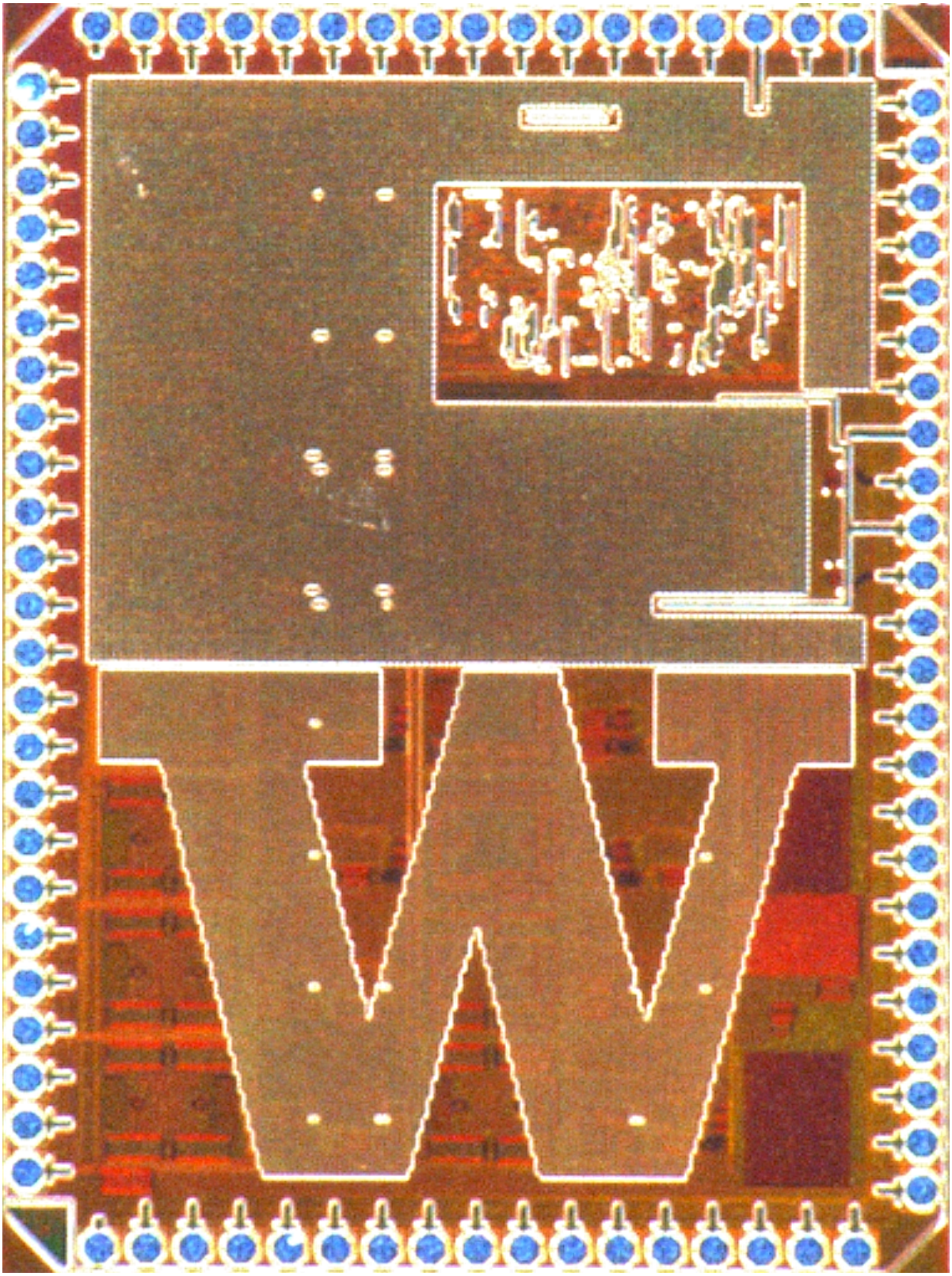

Figure 4.5: (2 x 2.7) mm^2 SoC.

Table 4.1: Power breakdown of SoC.

Mode	RF	AFE	ADC	Digital	μController	Total
12-Lead ECG	594 μW	368.8 μW	8 μW	10.2 μW	7.9 μW	984 μW
HR Monitor	0.5 μW	31 μW	8 μW	7.5 μW	48 μW	95 μW

4.1.5 Acknowledgements

The authors would like to thank Dr. Lawrence Sherman, M.D. for providing ECG expertise, Stratos for assistance in garment modification and Jeremy Lawrence for ECG display software.

4.2 Additional Applications

The above biosignal monitoring device was originally deployed in human heart monitoring applications. However, the high level of configurability means this device is well suited for many more diverse applications. Next we will discuss two additional applications for the monitoring device, a theoretical EEG system and a fully-deployed EMG system.

4.2.1 EEG

Electroencephalography (EEG) is the recording of electrical potentials on the surface of the scalp generated by groups of neurons in the brain firing. The potential generated by a single neuron is too small to be measured with EEG due to attenuation between the brain and the scalp but groups of neurons firing in unison will provide a measurable voltage at the scalp due to superposition with these multiple potentials summing. Filtering from the brain to the scalp as well as this superposition requirement change the signal morphology greatly from a single neuron. Typically EEG signal amplitudes range from 10-100 μV and most of the power is located between 0.5-100 Hz with many recording devices using a low-pass cutoff of

Table 4.2: Comparison to prior ECG textiles.

	This Work	**Yan (JSSC'11)**	**Yoo (JSSC'10)**	**Buxi (Bio-CAS'12)**
Sensors	ECG	ECG, TIV	ECG	ECG, ETI, Accelerometer
Wearable	shirt with dry electrodes	chest bandage	chest strap	wired electrodes
Active Power	984 μW	2.9 mW	5.2 mW	4.4 mW
Encryption	128 AES	none	128 AES	none
ECG Input Referred Noise	66 nV/$\sqrt{Hz}$	58 nV/$\sqrt{Hz}$	47 nV/$\sqrt{Hz}$	110 nV/$\sqrt{Hz}$
Communication	433 MHz FSK	13 MHz Body Channel	Wired	2.4 GHz GFSK
Wireless Range	$\sim$10 m	on-body	N/A	not stated
Data Rate	200 kbps	1 Mbps	x	30 kbps
Clinical 12-Lead ECG	yes	no	no	no
Sample Rate/ch	1.52 kS/s	0.5 kS/s	not stated	0.5 kS/s
Technology	0.13 μm	0.18 μm	0.18 μm	off-the-shelf
Note	Dry electrodes, no surface prep required	Duty cycled 5 % for 200 μW average power and 5 kbps effective datarate	Sensors inductively couple to battery powered strap logging data	Custom IC for analog front end/processing with commercial radio

35-70 Hz. [46][47]. Modern EEG uses digital sampling at a rate of usually at least 256 Hz.

Wireless EEG requires that all recorded data is transmitted over-the-air using an on-board power source (e.g. battery). Assuming a 10 bit analog-to-digital converter (ADC) is doing the sampling a wireless system must transmit data greater than (2.56 x num. channels) kbps where very generally higher data rates result in higher power consumption, which requires a large battery or causes short recording lifetime. To save power, reduce battery size or limit electrode complexity many wireless EEG systems reduce their channel counts compared to clinical wired systems.

Currently Available Systems

There are various wireless EEG systems along with display/signal processing software currently available, some commercially available for purchase and others developed within the research community, which can be accessed via partnerships and licensing avenues. Most of the commercial products are focused on brain-computer interfaces and feature additional sensors such as gyroscopes to monitor head position and electrooculography (EOG) to track eye movement. These systems tend to have a limited number of EEG channels because of their consumer-oriented focus (gaming control, focus group monitoring, etc.).

Two commercially available wireless EEG systems that are viable for research-quality recordings are the B-Alert X Series Mobile EEG [48] and the Emotive EPOC EEG system [49]. B-Alert offers 3, 9 or 20 channel wireless EEG variants with at least one optional channel for non-EEG recording (ECG, EMG, etc.). These also employ an accelerometer to track head position. Each variant offers over 6 hours of battery lifetime, with the battery size increasing with the larger channel options. Data is wirelessly transmitted via Bluetooth to a PC using a supplied receiver for signal processing and display. The Emotive EPOC similarly is a 14-channel wireless EEG with an on-board gyroscope to track head position and claims a battery life of 12 hours. The data is transmitted to a PC attached with a USB wireless receiver dongle.

A fairly complete 8-channel wireless EEG system has been developed at Imec for their Hu-

man++ project [50][51]. This design uses custom electronics to reduce power consumption, resulting in 22 hours of battery life in a smaller footprint compared to the commercial systems. This design also uses custom dry electrodes that do not require surface preparation. Access to this device requires enrollment in Imecs Human++ program as a research partner or with a separate licensing agreement.

Comparison

Table 4.3 shows a summary of the main points of comparison between the wireless EEG systems along with the same specifications for the 12-channel wireless sensor chip described in this chapter. The Emotiv system has a lower than standard sampling rate which makes this system unsuitable for EEG recordings for signal characteristics above 45Hz; the other two systems have sufficient bandwidth. The 19-channel B-Alert system has a large battery pack attached to the back of the head while both Emotiv and Imec have smaller integrated batteries. B-Alert appears to have the highest noise floor however their data on this is a bit unclear.

In comparison to these currently available EEG systems the custom IC discussed in this chapter appears to be highly competitive. The 12 channels of recording are application agnostic, equally suitable to EEG recordings as they are for ECG in the smart shirt implementation. With a sampling rate in 12-channel mode of 1.52 ksps there is no risk of aliasing the EEG signals and easily beats the other EEG systems discussed here. The 24 hour lifetime calculated for this IC is comparable to other systems but is using the small 11.5 mm diameter coin cell battery. Increasing the battery size, easily done in the EEG head-mounted form factor, would extend lifetime even further.

4.2.2 EMG

Building off of the work in [1][25] the IC presented here was also used for on-skin human EMG recording. In collaboration with the Center for Sensorimotor Neural Engineering (CNSE) the chip was imbedded in a custom sleeve. This sleeve is outfitted with 12 sets of EMG

Table 4.3: Comparison of Systems.

	B-Alert	Emotiv	Imec	**This Work**
EEG Channels	3-19	14	8	12
Sampling Rate/Ch	256 Hz	128 Hz	1024, 512 or 256 Hz	1.52 kHz
EEG Bandwidth	0.1-100 Hz	0.2-45 Hz	0.5-375, 210 or 128 Hz	0.1-750 Hz
Input Referred Noise	$630\,\mathrm{nV}/\sqrt{Hz}$	Not Stated	$66\text{-}77\,\mathrm{nV}/\sqrt{Hz}$	$66\,\mathrm{nV}/\sqrt{Hz}$
Signal Resolution	2000 nV	510 nV	244 nV	39 nV
Orientation Tracking	Yes	Yes	No	No
Battery Lifetime	6 hours	12 hours	Up to 22 hours	24 hours
Surface Prep	Required	Required	Optional	Unknown
Impedance Monitoring	Yes	Yes	Yes	No

electrodes made of a conductive fiber. Together with the IC this sleeve can perform fully wireless EMG recording from 12 separate locations on a human forearm and bicep.

Figure 4.6 shows the entire system. Included with the sleeve are the custom wireless receiver (described in [25]), a PC for live processing of EMG data and an infrared sensor to detect physical arm movement and location. Together this system is able to play a more advanced version of the therapeutic video game described in [1].

Using 12 channels for EMG recording as opposed to 2 in [1] brings about some significant advantages. With more channels EMG electrodes can fully surround the forearm instead of 1 electrode pair each specially placed for flexor and extensor groups. With electrodes surrounding the whole forearm the user can then be instructed to perform specific motions while wearing the sleeve. With this data recorded the PC can then process the data and determine with high confidence exactly where the electrodes of each channel are placed.

This eliminates the need for an expert to specially place each electrode, instead the user can perform this task autonomously. Figure 4.7 shows the recorded EMG of all 12 channels simultaneously from a user while flexing specific muscle groups in a predefined sequence.

Additionally, by averaging two adjacent channels together with different weights we can create "virtual" EMG signals to read from a specific location even if the physical electrodes are not there. This concept is similar to the virtual ECG leads presented in [43]. The highly configurable nature of this IC allows for simple insertion of the EMG electrode sleeve. Only gain and filter frequency modification were required to transition from ECG mode to EMG. All of the advantages of the circuit for ECG applications, notably reduced size , low-power operation and up to 20 m range, apply to this EMG system.

Figure 4.6: Full arm EMG sensing system utilizing custom IC. Sleeve is turned inside out to show EMG electrodes.

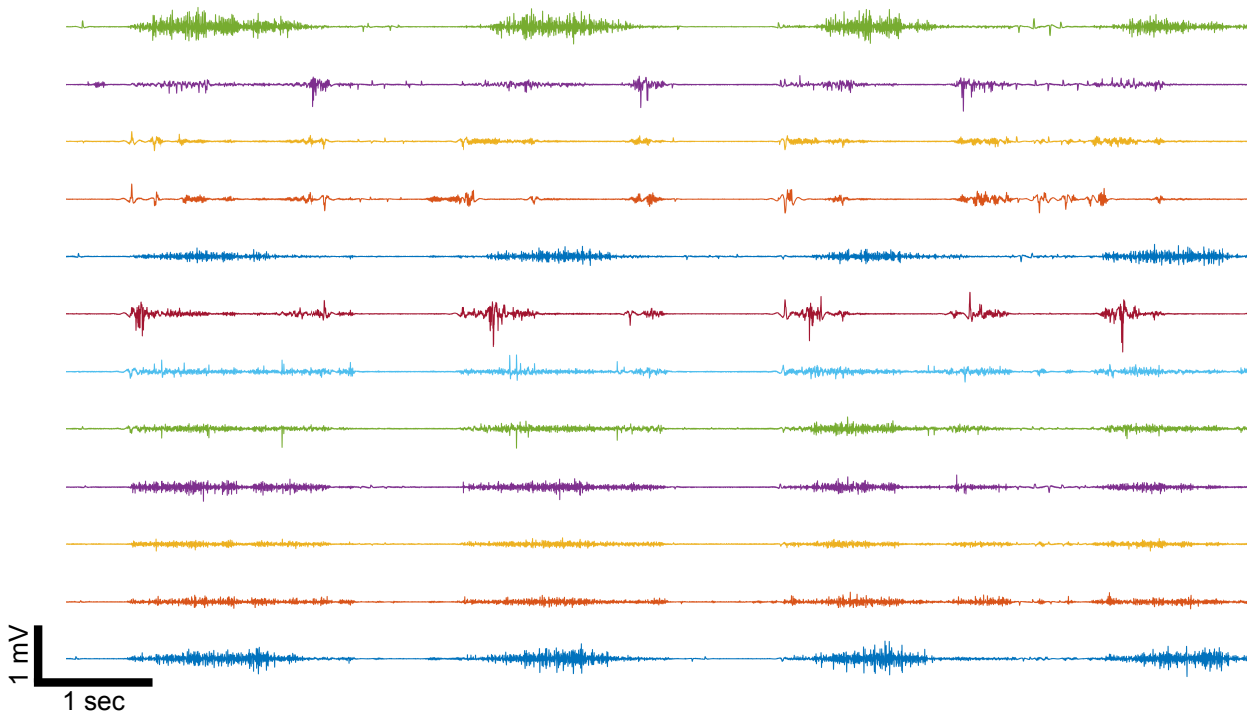

Figure 4.7: 12-channel EMG from the custom sensor sleeve recording from a human patient while periodically flexing the bicep muscle group.

Chapter 5

CONCLUSION

Advances in electronic device design have had significant benefits to biosignal monitoring. It is now possible to create devices small enough for applications previously thought impossible. One key driver for this reduction in size is the application of custom integrated circuits where low-power operation can be a key design constraint. With reduced power comes reduced battery-size if device lifetime is held constant.

In Chapter 2 we first introduce a two channel wireless EMG device created using only commercially-available components. This device, while capable of accurate EMG monitoring for over 10 hours, takes up over $6\,\mathrm{cm}^3$ per channel. By contrast, the second EMG device presented in Chapter 2 takes advantage of a custom IC as its backbone. The advantages of tight feature integration and low-power design allows this device to take up less thank $1\,\mathrm{cm}^3$ and operate for almost 3 days. By comparing these two devices with similar functionality the benefits of a design utilizing custom ICs, in this case enabling an over $6X$ decrease in size while at the same time increasing operational lifetime by $5X$.

Next we showed a custom four channel wireless biosignal monitor device with a custom IC at its heart. Again, the highly power-optimized circuit design here allows the entire system to fit in a form factor under $1\,\mathrm{cm}^3$. This small size allows it to be deployed in extremely size and weight constrained environments such as on freely moving mice for neural recording and freely moving moths for EMG while still having full-day lifetime from a single battery. The device itself was designed to simplify user interactions, hardwiring default AFE setting which can later be changed via an IR remote interface. Customizing the IC logic to simplify the user interface requires advanced knowledge of the final application. Because of this the device is limited to use in applications that require continuous sampling and wireless transmission

of one to four biosignal channels.

Developing a new IC takes a significant amount of engineering time. From conception to implementation it can easily take a year or more to create a new IC specifically for a new application. The final device introduced in Chapter 4 takes advantage of an IC design that aims to eliminate this long development time needed for a new IC by being more future-proof. For wireless biosignal monitoring applications the key pieces of a device remain the same: signal amplification, digitization and wireless transmission. This new IC design modularizes the internal blocks and provides for external control via a microcontroller allowing this IC to drastically change functionality, even in ways not envisioned during the IC design stage.

Using this final wireless biosignal monitoring device a "smart shirt" was developed. Thanks to the small size afforded by the combined functionality and low power of the IC this shirt has fully embeded the biosignal monitor along with 10 fabric electrodes. It is capable of recording clinically relevant 12-lead ECG from a freely-moving human subject. Since the device is highly customizable in conjunction with a mated microcontroller this same smart shirt can transition from 12-lead ECG to an extremely low power heart rate monitor. To further demonstrate the flexibility of this design possible applications in EEG were discussed and a "smart sleeve" EMG application was also demonstrated.

Leveraging the highly customizable nature of custom integrated circuits is an extremely powerful design tool for biosignal monitoring devices. The ability to limit functionality to only the needed circuitry and highly optimize the included circuits significantly drives down overall device size. This reduced size has enabled deployment in size constrained applications, such as on freely-moving mice and seamlessly embedded into garments for human use.

However, the strongest feature of this device is its reprogrammability using a microcontroller. Most biosignal monitoring applications require the same circuitry for amplification, digitization and transmission. Instead of each new application requiring a new chip design, one that re-uses these blocks but with new application-specific control logic, this device can individually control these building block circuits with the aid of a programmable microcontroller to completely change chip functionality with the same IC. This modular design with

external control is extremely powerful, making the chip useful for many more applications than were even foreseen during design. Instead of designing an IC for each deployment we can now simply reprogram a microcontroller for entirely new functionality, drastically reducing the design time for a new application and greatly increasing the deployment opportunities of the device.

Biosignal monitoring is becoming more and more prevalent in everyday life. Technologies like the ECG monitoring smart shirt are capable of continuously monitoring a patient's vital signals without any outside intervention. This automated approach of directly monitoring health metrics, as opposed to relying on the patient to report any perceived issues, has the potential to drastically reduce delays between the first physiological signs of health issues and alerting medical professionals for immediate care. Studies have shown that reducing the time-to-care for out-of-hospital cardiac arrest events from 15 minutes to 5 minutes could almost double the survivability rate of these events [52], an application the ECG shirt is directly targeted at. Early detection devices, not only this smart shirt for heart monitoring but many other human health monitoring devices, could drastically increase the survivability rate of many common diseases simply by alerting medical professionals at the earliest sign of trouble.

To make this vision a reality these devices must be unobtrusive enough that the general populous would deem them acceptable for daily wear. A major hurdle in creating all these small monitoring devices is the design time required for each one. The final IC presented here uses an architecture designed to combat this and enable easy deployment of all manor of life-saving devices. If these devices become common enough perhaps human death due to lack of immediate medical care can become a relic of the past.

BIBLIOGRAPHY

[1] C. Moritz, T. Morrison, B. Otis, J. Burt, D. Rios, T. Gilbertson, and S. McCoy, "'Neurogame Therapy' for Improvement of Movement Coordination after Brain Injury: Developing a Wireless Biosignal Game Therapy System," *IEEE Global Humanitarian Technology Conference*, 2011. p. 72-77.

[2] N. Bradley and S. L. Westcott, "Motor Control: Developmental Aspects of Motor Control in Skill Acquisition," *Pediatric Physical Therapy, 3rd Ed.*, S.K. Campbell, Editor. 2006. p. 77-130.

[3] K. H. Kong, K. S. Chua, and J. Lee, "Symptomatic upper limb spasticity in patients with chronic stroke attending a rehabilitation clinic: frequency, clinical correlates and predictors," *J Rehabil Med*, 2010. 42(5): p. 453-7.

[4] A. C. Eliasson, et al., "Development of hand function and precision grip control in individuals with cerebral palsy: a 13-year follow-up study," *Pediatrics*, 2006. 118(4): p. e1226-36.

[5] M. Franceschini, et al., "Is health-related-quality of life of stroke patients influenced by neurological impairments at one year after stroke?," *Eur J Phys Rehabil Med*, 2010. 46(3): p. 389-99.

[6] A. M. Gordon, et al., "Efficacy of a hand-arm bimanual intensive therapy (HABIT) in children with hemiplegic cerebral palsy: a randomized control trial," *Dev Med Child Neurol*, 2007. 49(11): p. 830-8.

[7] L. Oujamaa, et al., "Rehabilitation of arm function after stroke. Literature review," *Ann Phys Rehabil Med*, 2009. 52(3): p. 269-93.

[8] M.L. Urton, et al., "Systematic literature review of treatment interventions for upper extremity hemiparesis following stroke," *Occup Ther Int*, 2007. 14(1): p. 11-27.

[9] Beekhuizen, K.S. and E.C. "Field-Fote, Massed practice versus massed practice with a stimulation: Effects on upper extremity function and cortical plasticity in individuals with incomplete cervical spinal cord injury," *Neurorehabilitation and Neural Repair*, 2005. 19(1): p. 33-45.

[10] Garvey, M.A., et al., "Cerebral palsy: new approaches to therapy," *Curr Neurol Neurosci Rep*, 2007. 7(2): p. 147-55.

[11] Johnston, M.V., "Plasticity in the developing brain: implications for rehabilitation," *Dev Disabil Res Rev*, 2009. 15(2): p. 94-101.

[12] Kleim, J.A. and T.A. Jones, "Principles of experience-dependent neural plasticity: implications for rehabilitation after brain damage," *J Speech Lang Hear Res*, 2008. 51(1): p. S225-39.

[13] Coleman, K.A. and J. Harry, "Development and Testing of a Novel EMG Feedback Technology to Induce Movement," *Neurology Report*, 2002. 26(2): p. 94-100.

[14] Coleman, K.A. and J. Harry, "Functional gait changes in patients with chronic lower extremity hemiplegia treated with a technology to induce movement (TIM)-type system," *Top Stroke Rehabil*, 2004. 11(4): p. 43-54.

[15] Goldstein, J., et al., "Video games and the elderly," *Social Behavior and Personality*, 1997. 25(4): p. 345-352.

[16] Nacke, L.E., A. Nacke, and C.A. Lindley, "Brain training for silver gamers: effects of age and game form on effectiveness, efficiency, self- assessment, and gameplay experience," *Cyberpsychol Behav,* 2009. 12(5): p. 493-9.

[17] Betker, A.L., et al., "Video game-based exercises for balance rehabilitation: a single-subject design," *Arch Phys Med Rehabil*, 2006. 87(8): p. 1141-9.

[18] Goude, D., S. Bjork, and M. Rydmark, "Game design in virtual reality systems for stroke rehabilitation," *Stud Health Technol Inform*, 2007. 125: p. 146-8.

[19] Bryanton, C., et al., "Feasibility, motivation, and selective motor control: virtual reality compared to conventional home exercise in children with cerebral palsy," *Cyberpsychol Behav*, 2006. 9(2): p. 123-8.

[20] Graves, L.E., N.D. Ridgers, and G. Stratton, "The contribution of upper limb and total body movement to adolescents' energy expenditure whilst playing Nintendo Wii," *Eur J Appl Physiol*, 2008. 104(4): p. 617-23.

[21] Rai, S., et al., "A 500μW Neural Tag with 2μVrms AFE and Frequency- Multiplying MICS/ISM FSK Transmitter," *IEEE International Solid-State Circuits Conference (ISSCC)*, 2009.

[22] Pandey, J. and B. Otis, "A Sub-100μW MICS/ISM Band Transmitter Based on Injection- locking and Frequency Multiplication," *IEEE Journal of Solid-State Circuits (JSSC)*, 2011: To appear.

[23] Pandey, J. and B. Otis, "A 90μW MICS/ISM Band Transmitter with 22% Global Efficiency," *IEEE Radio Frequency Integrated Circuits (RFIC)*, June 2010: p. 285-288.

[24] Pandey, J., J. Shi, and B. Otis, "A 120μW MICS/ISM-Band FSK Receiver with a 44μW Low-Power Mode Based on Injection-Locking and 9x Frequency Multiplication," *IEEE International Solid State Circuits Conference (ISSCC)*, February 2011.

[25] T. Morrison, M. Nagaraju, B. Winslow, A. Bernard and B. P. Otis, "A 0.5 cm^3 Four-Channel 1.1 mW Wireless Biosignal Interface With 20 m Range," *"IEEE Trans. Biomed. Circuits Syst."*, Vol. 8, no. 1, pp. 138–147, February 2014.

[26] D. Yeager, J. Holleman, R. Prasad, J. R. Smith, and B. P. Otis, "NeuralWISP: A wirelessly powered neural interface with 1-m range," *"IEEE Trans. Biomed. Circuits Syst."*, Vol. 3, no. 6, pp. 379–387, October 2009.

[27] R. R. Harrison, H. Fotowat, R. Chan, R. J. Kier, A. Leonardo, and F. Gabbiani, "A wireless neural/EMG telemetry system for freely moving insects," in *Proc. IEEE Intl. Symp. Circuits Syst.*, Paris, France, June 2010, pp. 2952–2955.

[28] D. Fan, D. Rich, T. Holtzman, P. Ruther, J. W. Dalley, A. Lopez, M. A. Rossi, J. W. Barter, D. Salas-Meza, S. Herwik, T. Holzhammer, J. Morizio, and H. H. Yin, "A wireless multi-channel recording system for freely behaving mice and rats," *PLoS ONE 6(7): e22033. doi:10.1371/journal.pone.0022033*, 2011.

[29] R. R. Harrison, H. Fotowat, R. Chan, R. J. Kier, R. Olberg, A. Leoardo, and F. Gabbiani, "Wireless neural/EMG telemetry systems for small freely moving animals," *"IEEE Trans. Biomed. Circuits Syst."*, Vol. 5, no. 2, pp. 103–111, April 2011.

[30] M. S. Chae, Z. Yang, M. R. Yuce, L. Hoang, and W. Liu, "A 128-channel 6 mW wireless neural recording IC with spike feature extraction and UWB transmitter," *"IEEE Trans. Neural Syst. Rehabil. Eng."*, Vol. 17, no. 4, pp. 312–321, August 2009.

[31] N. V. Helleputte, S. Kim, H. Kim, J. P. Kim, C. V. Hoof, and R. F. Yazicioglu, "A 160μA biopotential acquisition ASIC with fully integrated IA and motion-artifact suppression," in *IEEE Int. Solid-State Circuits Conf. Dig. Tech. Papers*, February 2012, pp. 118–120.

[32] F. Inanlou, M. Kiani, and M. Ghovanloo, "A 10.2 Mbps pulse harmonic modulation based transceiver for implantable medical devices," *"IEEE J. Solid-State Circuits"*, Vol. 46, no. 6, pp. 1296–1306, June 2011.

[33] C. Hu, R. Khanna, J. Nejedlo, K. Hu, H. Liu, and P. Y. Chiang, "A 90 nm-CMOS, 500 Mbps, 3-5 GHz fully-integrated IR-UWB transceiver with multipath equalization using pulse injection-locking for receiver phase synchronization," *"IEEE J. Solid-State Circuits"*, Vol. 46, no. 5, pp. 1076–1088, May 2011.

[34] M. Azin, D. J. Guggenmos, S. Barbay, R. J. Nudo, and P. Mohseni, "A battery-powered activity-dependent intracortical microstimulation IC for brain-machine-brain interface," *"IEEE J. Solid-State Circuits"*, Vol. 46, no. 4, pp. 731–745, April 2011.

[35] R. R. Harrison and C. Charles, "A low-power low-noise CMOS amplifier for neural recording applications," *"IEEE J. Solid-State Circuits"*, Vol. 38, no. 6, pp. 958–965, June 2003.

[36] S. Rai, J. Holleman, J. Pandey, F. Zhang, and B. Otis, "A 500μW neural tag with 2μVrms AFE and frequency-multiplying MICS/ISM FSK transmitter," in *IEEE Int. Solid-State Circuits Conf. Dig. Tech. Papers*, February 2009, pp. 212–213.

[37] J. Holleman and B. Otis, "A sub-microwatt low-noise amplifier for neural recording," in *Engineering in Medicine and Biology Society, 2007. EMBS 2007. 29th Annual International Conference of the IEEE*, August 2007, pp. 3930–3933.

[38] A. Rush and P. R. Troyk, "Power and data for a wireless implanted neural recording system," in *Neural Engineering (NER), International IEEE/EMBS Conference on*, April 2011, pp. 507–510.

[39] R. L. Rennaker, J. Miller, H. Tang, and D. A. Wilson, "Minocycline increases quality and longevity of chronic neural recordings," *Journal of Neural Engineering*, Vol. 4, no. 2, pp. L1–5, June 2007.

[40] R. L. Rennaker, S. Street, A. M. Ruyle, and A. M. Sloan, "A comparison of chronic multi-channel cortical implantation techniques: manual versus mechanical insertion," *Journal of Neuroscience Methods*, Vol. 142, no. 2, pp. 169–176, March 2005.

[41] J. Lubke and D. Feldmeyer, "Excitatory signal flow and connectivity in a cortical column: focus on barrel cortex," *Brain Structure and Function*, Vol. 212, no. 1, pp. 3–17, 2007.

[42] R. Q. Quiroga, Z. Nadasdy, and Y. Ben-Shaul, "Unsupervised spike detection and sorting with wavelets and superparamagnetic clustering," *Neural Computation*, Vol. 16, pp. 1661–1687, 2004.

[43] T. Morrison, J. Silver, and B. Otis, "A Single-chip Encrypted Wireless 12-Lead ECG Smart Shirt for Continuous Health Monitoring," *IEEE Symp. on VLSI Circuits*, 2014.

[44] M. Pedley, et al.. (2013). Available: http://www.smartlifetech.com/technology/Health-Vest-/

[45] 2XU. (2013). "Mens Elite Golf L/S Compression Top." Available: http://www.2xu.com/product/983/Mens-Elite-Golf-LS-Compression-Top/261/264

[46] Niedermeyer, E., and da Silva, F.L. "Electroencephalography: Basic Principles, Clinical Applications, and Related Fields," *Lippincot, Williams and Wilkins*, 2004.

[47] Aurlien, H et al., "EEG background activity described by a large computerized database". *Clinical Neurophysiology 115 (3)*, 2004. p. 66573.

[48] *http://advancedbrainmonitoring.com/xseries/*

[49] *http://www.emotiv.com/eeg/features.php*

[50] Brown, L.,van de Molengraft, J., Yazicioglu, R.F., Torfs, T., Penders, J., Van Hoof, C., "A low-power, wireless, 8-channel EEG monitoring headset," *Engineering in Medicine and Biology Society (EMBC)*, pp.4197-4200, Aug. 2010.

[51] *http://www2.imec.be/be_en/press/imec-news/imeceeg2012.html*

[52] Pell, J.P., Sirel, J.M., Marsden, A.K., et al. "Effect of reducing ambulance response times on deaths from out of hospital cardiac arrest: cohort study." BMJ 2001;322:13858.